Preparatory Modelling Week, September 7–14, 2015, Sofia, Bulgaria

Group 2

Axisymmetric Drop Shape Analysis

Galina Lyutskanova

Faculty of Mathematics and Informatics, Sofia University,
g.lyutskanova@gmail.com

Kiril Mihaylov

Faculty of Mathematics and Informatics, Sofia University,
kirilmihaylov94@gmail.com

Vasil Kolev

Institute of Information and Communication Technologies, BAS,
kolev_acad@abv.bg

Instructor: **Tihomir Ivanov**

Faculty of Mathematics and Informatics, Sofia University,
tbivanov@fmi.uni-sofia.bg

Abstract. In the present work, we develop an algorithm for the real-time estimation of the surface tension of an axisymmetric drop, subjected to gravitational or rotational forces. We propose an edge detection algorithm that gives an experimental profile from an image of a drop. Then we derive mathematical models for both cases based on the Young–Laplace equation of capillarity. We solve them by using the Euler and the fourth order Runge–Kutta methods and obtain corresponding theoretical profiles. Based on that, we estimate the surface tension so that the theoretical and experimental profiles coincide. For this purpose we use two optimization algorithms, namely the Gauss-Newton and the Deepest descent methods.

2.1 Introduction

The goal of the present work is to derive an algorithm for obtaining the surface tension of a fluid, using the geometry of a drop of the fluid.

Measuring surface tension gives information on a range of material properties, e.g. absorption and adsorption properties, cleanliness, spreading, surface free energy, surface heterogeneity, and wettability. These properties are important in studying and developing or controlling the quality of engineered surfaces and technical liquids. Thus, the surface tension is used in a great variety of industries such as biomaterials, chemicals, pharmaceuticals, electronics, foods, energy, environment, paper and packaging with applications ranging from determining the surface properties of contact lenses to the quality control of semiconductors. For measuring surface tension, tensiometers (Fig. 2.1) are used. One of the main

Figure 2.1: Optical tensiometer, using pendant drops method [6]

approaches that those devices use is the Axisymmetric Drop Shape Analysis (see Fig. 2.2). It consists of the following steps.

Step 1. First a drop is created, using some kind of an optical tensiometer.

1. A pendant drop (Fig. 2.3a) is a drop suspended from a needle in a bulk liquid or gaseous phase. The shape of the drop is a result from the interaction between the surface tension and the pressure due to gravity.

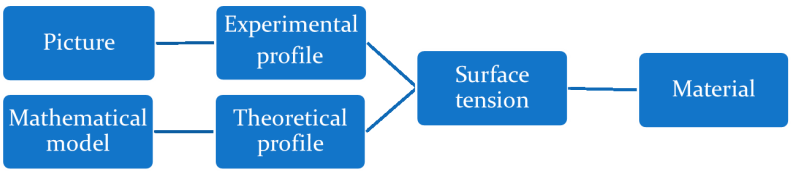

Figure 2.2: Schematic representation of ADSA

2. A sessile drop (Fig. 2.3b) is a drop that comes from a capillary, perpendicular to the ground. The shape of the drop is once again a result from the interaction between the surface tension and the pressure due to gravity.

3. A spinning drop (Fig. 2.3c) is created in a horizontally arranged rotating tube filled with a bulk phase. The forces that act on it are the gravitational force, centrifugal force, and the forces due to the surface tension and the internal (external) pressure.

(a) Pendant drop [1] (b) Sessile drop [7] (c) Spinning drop [8]

Figure 2.3: Types of drops

Step 2. An image of the drop is captured using a camera and the drop's profile is extracted, using an edge detection algorithm. Thus, we obtain an experimental profile of the drop.

Step 3. Using the Young-Laplace equation of capillarity, we obtain a mathematical model (ODE system), depending on 2 parameters. The solution of the model with fixed parameters is called a theoretical profile.

Step 4. Finally, we estimate the values of the model parameters that minimize the distance between the theoretical and experimental profiles and, thus, estimate the surface tension (it is contained in one of the two parameters).

This approach has been extensively studied in the literature. Here, we shall mention just a few works on the subject. In [3], Rotenberg, Boruvka, and Neumann derived the model of the drop. In [1], Hoorfar and Neumann described methods for measuring contact angles from the volume and diameter of versatility for sessile and pedant drops. In [4], advanced numerical methods have been used to improve the numerical stability and global convergence. They are applicable to pendant and sessile drops.
Independent of the specific settings of the experiment, our approach will be the same. In section 1, we explain how we will obtain the cloud of points of the drop's contour. In section 2, we will derive a model, based on the Young-Laplace equation of capillarity. There will be some differences in the model, depending on the type of drop. In section 3, we will derive numerical schemes for solving the model equations based on the Euler and Runge-Kutta methods. In section 4, we will use the Deepest descent and Gauss-Newton methods to obtain the parameters,

minimizing the distance between the theoretical and the experimental profiles. In the Appendix, some mathematical and physical concepts are introduced, i.e. pressure, surface tension, and curvature that are needed for deriving the model of the drop.

2.2 Edge detection

As we said, first we have an image of a drop, taken from an apparatus, and we must find the contour of the drop. We assume that the drop is an axisymmetric three-dimensional object and, thus, it is sufficient to work with its two-dimensional projection. Let us introduce the coordinate system Oxz.

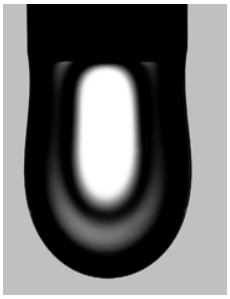

Figure 2.4: An image of a pendant drop taken from a camera

We make the following assumptions about the image.

1. It is a grayscale image with lighter fone color and a drop with contrasting dark color.

2. The tube is straight with no disruptions.

We propose the following algorithm for the edge detection, based on a threshold, δ. We shall illustrate it using the image shown in Fig. 2.4.
Step 1. Make the image black and white, so that the drop is black and the fone is white.

We initialize the first pixel on the first row, i, with white color. If the absolute value of the difference between the pixel i and any other pixel j in the picture is less than δ, then the pixel j is set to white. Otherwise, it is set to black (see Fig. 2.5).

Figure 2.5: Image obtained after step 1 of the edge detection algorithm with $\delta = 40$ (if δ is smaller, e.g. 10, we get really curly border) .

Step 2. Select the first black pixel from every row to obtain the left half of the

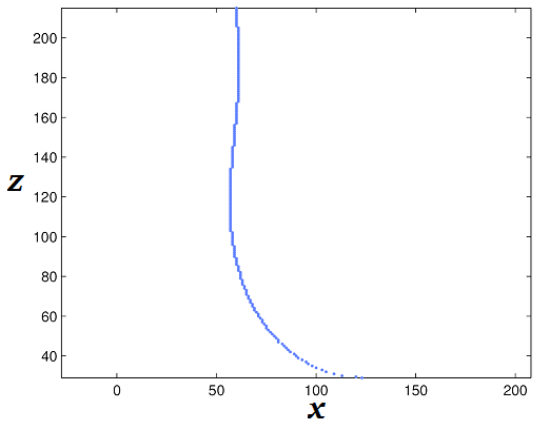

Figure 2.6: Image obtained after step 2 of the algorithm.

contour of the drop, see Fig. 2.6.

Step 3. We translate the drop so that the apex goes to the origin and flip it around the z-axis. We cut the tube easily, because of assumption 2 — we remove all the pixels starting from the first row of the picture with the same x-coordinate. We add a point that is the real point of the apex (it is obtained by taking the middle between the first black pixel and the last black pixel in a chosen row). Finally, at this step we rescale the image, so that the first point in it is with x-coordinate equal to 1.

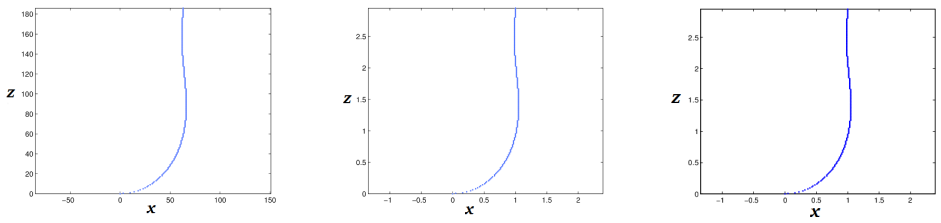

(a) Translation, reflection (b) Cutting the pipe (c) Rescaling the picture

Figure 2.7: Step 3 of the algorithm.

The result of the algorithm for another image of a pendant drop is shown at Fig. 2.8.

For **sessile drops** we make some modifications of the algorithm. If the drop is sessile, before step 1 of the algorithm, we flip the image around the x-axis. Then, finally, after step 3, we make a reflection of the image with respect to the x-axis.

The results, produced by the algorithm for sessile and rotating drops, are shown at Fig. 2.9 and Fig. 2.10.

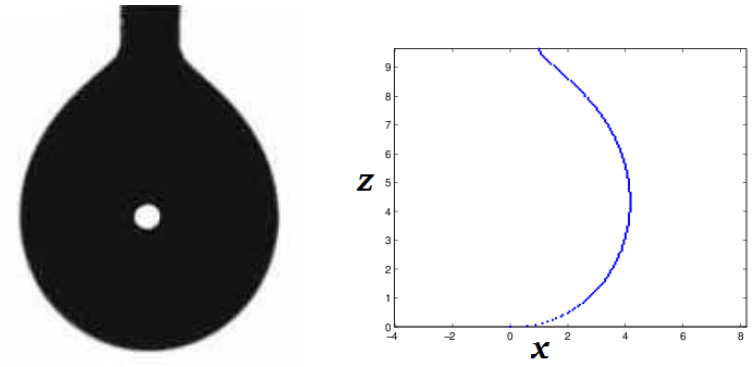

(a) Initial pendant drop [7] (b) Final profile

Figure 2.8: Edge detection for an image of a pendant drop

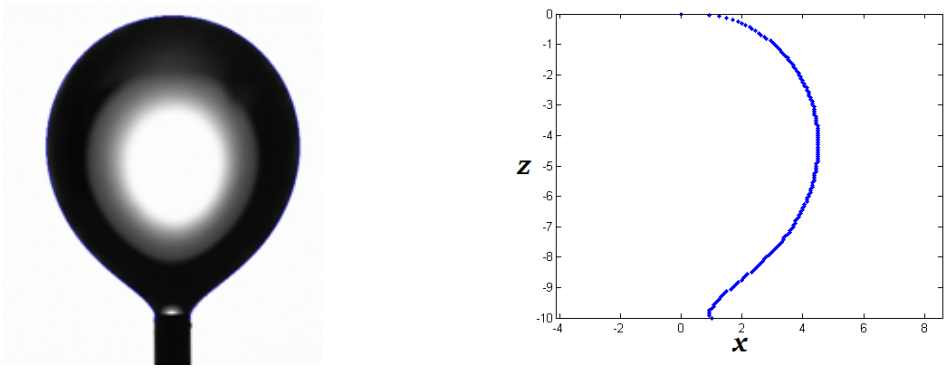

(a) Initial sessile drop (b) Final profile

Figure 2.9: Edge detection for a sessile drop

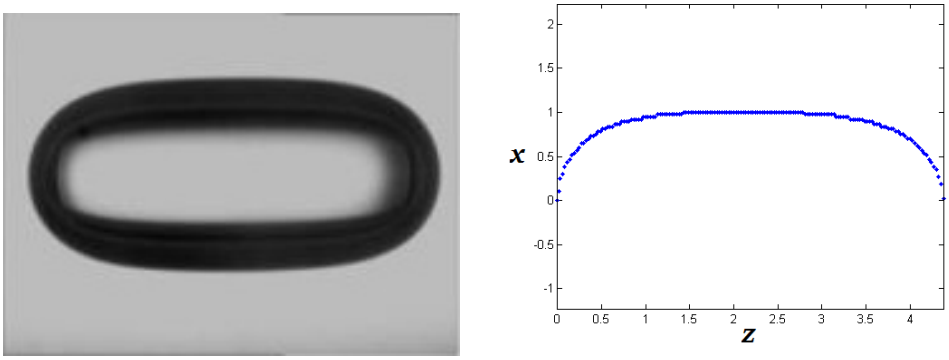

(a) Initial rotating drop (b) Final profile

Figure 2.10: Edge detection for a rotating drop

2.3 Mathematical Model

2.3.1 Young–Laplace equation of capillarity

The Young–Laplace equation of capillarity (cf. [3]) describes the relation between the mean curvature of a drop (i.e., its geometry), the pressure, induced in it, and the surface tension.

Let us consider an infinitesimally small part $ABCD$ of the surface of a fluid, where $\overset{\frown}{AB} = x$, $\overset{\frown}{BC} = y$ and $P \in ABCD$. Let the surface expand isotropically under some internal pressure, so that the points A, B, C, D, and P are projected to A_1, B_1, C_1, D_1, and P_1, respectively, and $PP_1 =: \Delta z$ (see Fig. 2.11). Let $\overset{\frown}{A_1B_1} = x + \Delta x$, $\overset{\frown}{B_1C_1} = y + \Delta y$. Since $ABCD$ is infinitesimally small, it can be

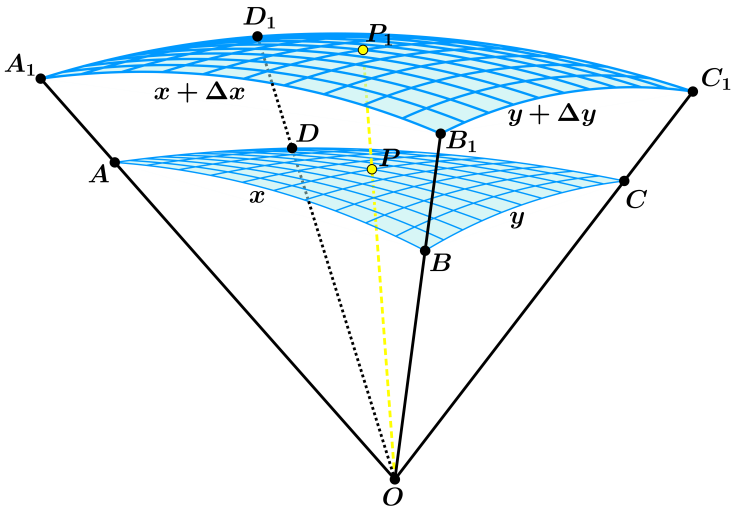

Figure 2.11: Expansion of an infinitesimally small part of a fluid.

approximated with a rectangle with dimensions x and y. Therefore, the area of its surface is

$$S_{old} = xy. \tag{2.1}$$

The area of $A_1B_1C_1D_1$ can be analogously written as

$$S_{new} = (x+\Delta x)(y+\Delta y) = xy + x\Delta y + y\Delta x + \Delta x\Delta y \approx xy + x\Delta y + y\Delta x. \tag{2.2}$$

In the latter, we have used the fact that Δx and Δy can be chosen to be arbitrarily small and, thus, $\Delta x\Delta y$ can be done negligibly small in comparison with $x\Delta y$ and $y\Delta x$.

Taking into account (2.1) and (2.2), it follows that the change of the area of the surface is

$$\Delta S = x\Delta y + y\Delta x \tag{2.3}$$

and the work ΔA due to the pressure is

$$\Delta A = \underbrace{(p_1 - p_2)}_{\Delta p} S_{old}\Delta z = \Delta p x y \Delta z. \tag{2.4}$$

Let R_1 and R_2 be the principal radii of curvature at the point P and O_1 and O_2 be the centers of the corresponding circles. Let $\overset{\frown}{EF}$ be the intersection between the circle with radius R_1 and $ABCD$ and let E_1 and F_1 be the central projections of E and F with center O (see Fig. 2.12). Because the neighborhood is infinitesimally small, we have $\overset{\frown}{EF} = x$ and $\overset{\frown}{E_1F_1} = x + \Delta x$. Let F_2 be the

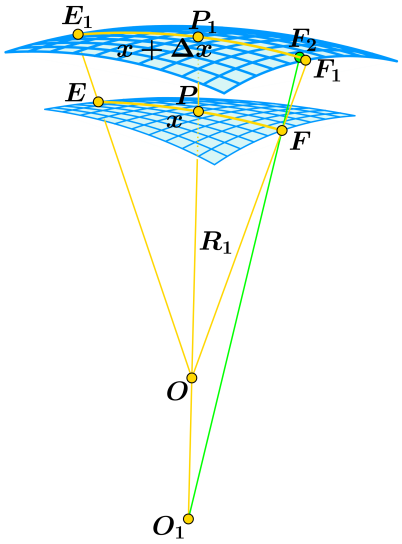

Figure 2.12: Central projection with center O_1.

central projection of F with center O_1. Because Δz is infinitesimally small, we can approximate $E_1F_2 = x + \Delta x$. Using the notation from Fig. 2.12, let us denote the angle between EO and FO with φ. Then, from the fact that $\varphi = \frac{\overset{\frown}{EF}}{R_1}$ and $\varphi = \frac{\overset{\frown}{E_1F_2}}{R_1+\Delta z}$, we obtain

$$\varphi = \frac{x}{R_1} = \frac{x + \Delta x}{R_1 + \Delta z} = \frac{\Delta x}{\Delta z},$$
$$\Delta x = \frac{x\Delta z}{R_1}.$$

Similarly, we can calculate that $\Delta y = \dfrac{y\Delta z}{R_2}$. We substitute Δx and Δy in (2.3) and obtain

$$\Delta S = \frac{x\Delta z}{R_1}y + \frac{y\Delta z}{R_2}x = xy\Delta z\left(\frac{1}{R_1} + \frac{1}{R_2}\right).$$

The pressure difference on the surface is compensated for by the surface tension, σ. The work due to σ (see the Appendix) is

$$\Delta A = \sigma\Delta S = \sigma xy\Delta z\left(\frac{1}{R_1} + \frac{1}{R_2}\right).$$

From the latter and (2.4), we obtain

$$\Delta p = \sigma \left(\frac{1}{R_1} + \frac{1}{R_2} \right), \tag{2.5}$$

which is called Young–Laplace equation of capillarity.

2.3.2 Derivation of the model for pendant drops

In order to derive the model from the Young–Laplace equation, we must find the mean curvature, H, and the pressure difference.

Mean curvature

Let us define an orthonormal coordinate system Oxz, where O is the apex of the drop and z is collinear with the axis of symmetry. We choose a point A from the drop's contour (see Fig. 2.13a) and through A we construct a plain α that is tangent to the drop's surface.

There exists a plain β that contains the point A and the axis of symmetry, which, without loss of generality, we can assume is the plain defined by the coordinate system. Because of the rotational symmetry, for all further analyses we shall consider β.

Let R_1 and R_2 be the principal radii of curvature at A and O_1 and O_2 be the centers of the corresponding circles. It can be shown that the normal line, n, to α lies in β and, thus, O_1 and O_2 lie in β (Fig. 2.13). In order to do so, we shall prove the following lemma.

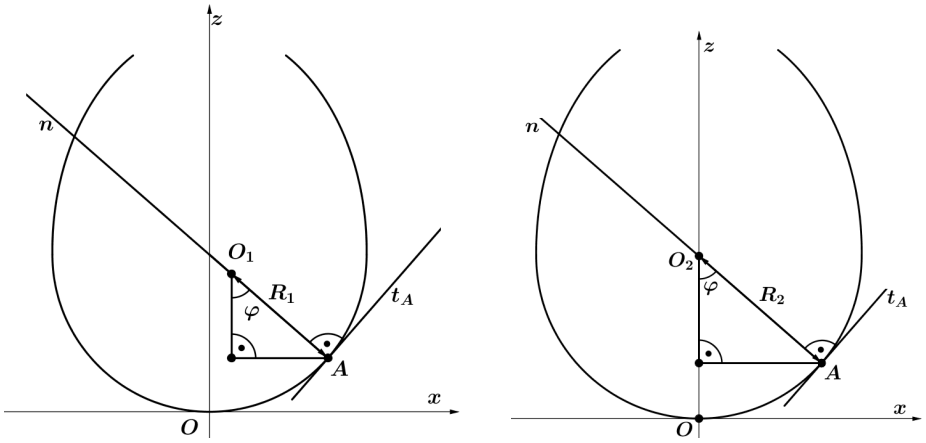

(a) First principal radius of curvature (b) Second principal radius of curvature

Figure 2.13: Principal radii of curvature

Lemma 1. *Let $z = f(x, y)$ be a surface having rotational symmetry, i.e. $z = f(r)$, where $r^2 = x^2 + y^2$. Then, the equality*

$$x \frac{\partial f(x,y)}{\partial y} = y \frac{\partial f(x,y)}{\partial x} \tag{2.6}$$

holds true.

Proof. Using the chain rule, for the partial derivatives of f we obtain

$$\frac{\partial f}{\partial x} = \frac{\partial f}{\partial r}\frac{\partial r}{\partial x} = \frac{\partial f}{\partial r}\frac{2x}{2(x^2+y^2)^{1/2}},$$
$$\frac{\partial f}{\partial y} = \frac{\partial f}{\partial r}\frac{2y}{2(x^2+y^2)^{1/2}}.$$

Multiplying the latter two equations with y and x, respectively, we obtain the desired equality. □

Now, we are ready to prove the following proposition.

Proposition 1. *The normal line, n, to α (the tangent plain to the drop's surface at A) lies in β (Fig. 2.13a).*

Proof. Let the drop's surface be described by the function $z = f(x, y)$ and let $A(x_0, 0, z_0)$ be a point on the surface. The normal to the surface at the point A has the form $(f_x(x_0, 0), f_y(x_0, 0), -1)$. We shall prove that it lies in Oxz, i.e. $f_y(x_0, 0) = 0$. Because the drop is axisymmetric, using Lemma 1, we obtain

$$\frac{\partial f(x_0, 0)}{\partial y} = 0,$$

which concludes the proof. □

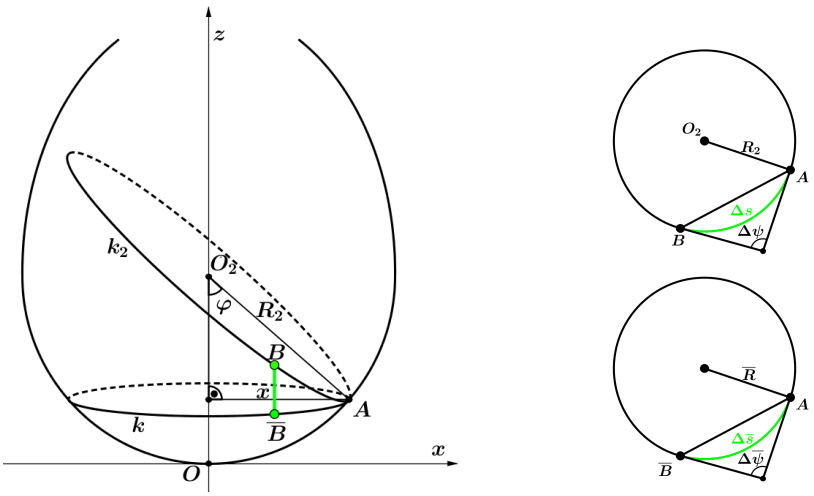

(a) The second principal center of curvature lies on the z-axis

(b) The second principal center of curvature and the cross section at point A

Figure 2.14: Second principal radius of curvature

Taking into account Proposition 1, the following can be shown.

Proposition 2. *Let A be an arbitrary point of an axisymmetric drop's contour. Then, the second principal center of curvature, O_2, is the intersection of the normal, n, to the surface and the z-axis.*

Proof. It is known that

$$R_2 = \lim_{\Delta\psi\to 0} \frac{\Delta s}{\Delta\psi} = \lim_{B\to A} \frac{\overset{\frown}{AB}}{\Delta\psi},$$

where B is a point from the principal circle of curvature (k_2), $\overset{\frown}{AB}= \Delta s$, and $\Delta\psi$ is the angle between the tangents to k_2 at A and B (see Fig. 2.14a and Fig. 2.14b). Let $\overline{B}$ be the orthogonal projection of B on the cross section, k, of the drop through A. Let $\overset{\frown}{A\overline{B}}= \Delta\overline{s}$. Then, we have

$$R_2 = \lim_{B\to A} \frac{AB}{\Delta\psi} = \lim_{\overline{B}\to A} \frac{A\overline{B}/\cos\theta}{\Delta\psi} = \frac{1}{\cos\theta} \lim_{\overline{B}\to A} \frac{\Delta\overline{s}}{\Delta\overline{\psi}} = \frac{1}{\cos\theta}\overline{R},$$

where θ is the angle between AB and $A\overline{B}$. We have used that $\lim\limits_{\overline{B}\to A} \frac{\Delta\psi}{\Delta\overline{\psi}} = 1$. We shall now prove it.

Let the radian measures of Δs and $\Delta\overline{s}$ be denoted by $\overset{\frown}{\Delta s}$ and $\overset{\frown}{\Delta\overline{s}}$, correspondingly. It is known that

$$\overset{\frown}{\Delta s} = \frac{\overset{\frown}{AB}}{R_2} = \frac{\overset{\frown}{A\overline{B}}\,/\cos\theta}{R_2},$$
$$\overset{\frown}{\Delta\overline{s}} = \frac{\overset{\frown}{A\overline{B}}}{x}.$$

Then, from Fig. 2.14b it is easy to see that

$$\Delta\psi = \pi - 2\frac{\overset{\frown}{\Delta s}}{2} = \pi - \frac{A\overline{B}/\cos\theta}{R_2},$$
$$\Delta\overline{\psi} = \pi - \frac{\overset{\frown}{A\overline{B}}}{x}$$

and, thus,

$$\lim_{\overline{B}\to A} \frac{\Delta\psi}{\Delta\overline{\psi}} = 1$$

holds true. Because the angle between AB and $A\overline{B}$ is θ, $R_2 \perp AB$ and $R \perp A\overline{B}$, the angle between R_2 and R is also θ. Hence, the angle between n and the z-axis is $\pi/2 - \theta$. Let us denote it by φ. Therefore, the following equality

$$\sin\varphi = \cos\theta = \frac{x}{R_2}$$

holds true. Because R_2 and n are collinear and $R_2 = \frac{x}{\cos\theta}$, then O_2 lies on the z-axis. □

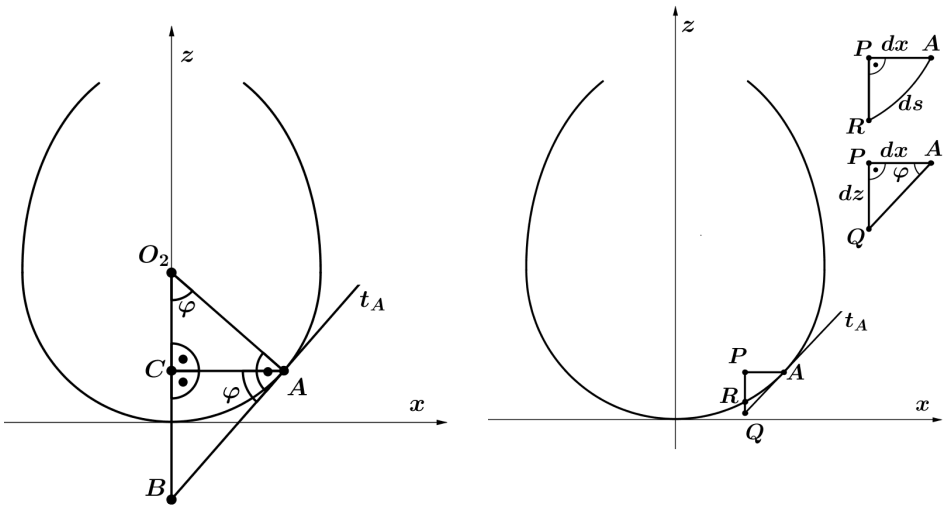

(a) The angle between the tangent line and the x-axis is φ.

(b) $dx/ds = \cos\varphi$
$dz/ds = \sin\varphi$

Figure 2.15: Meridional cross-section of the drop's surface.

Using the definition of curvature (B.4) and Proposition 2, we obtain

$$\frac{1}{R_1} = \frac{d\varphi}{ds}, \tag{2.7}$$

$$\frac{1}{R_2} = \frac{\sin\varphi}{x}. \tag{2.8}$$

Finally, we substitute (2.7) and (2.8) into (2.5) and rewrite the obtained differential equation as a first order ODE system. It is obvious that the angle between the x-axis and the tangent t_A at the point A is φ (Fig. 2.15a). Moreover, we can approximate the length of the segment AQ with the length of the arc ds and $\angle PAQ$ with $\angle PAR$, if ds is moving towards 0 (i.e. A is moving towards Q). Using the Sine theorem in $\triangle APR$ (see Fig. 2.15b), we obtain

$$\frac{dx}{ds} = \cos\varphi. \tag{2.9}$$

Analogously,

$$\frac{dz}{ds} = \sin\varphi. \tag{2.10}$$

Using (2.5), (2.7), (2.8), (2.9) and (2.10), we obtain the system

$$\begin{aligned} \frac{dx}{ds} &= \cos\varphi, \\ \frac{dz}{ds} &= \sin\varphi, \\ \frac{d\varphi}{ds} &= \frac{\Delta p}{\sigma} - \frac{\sin\varphi}{x}. \end{aligned} \tag{2.11}$$

Pressure difference

The optical tensiometer produces a drop in a container full of liquid (Fig. 2.16). We need to find the pressure difference $\Delta p = p_{out} - p_{in}$, where p_{out} is the

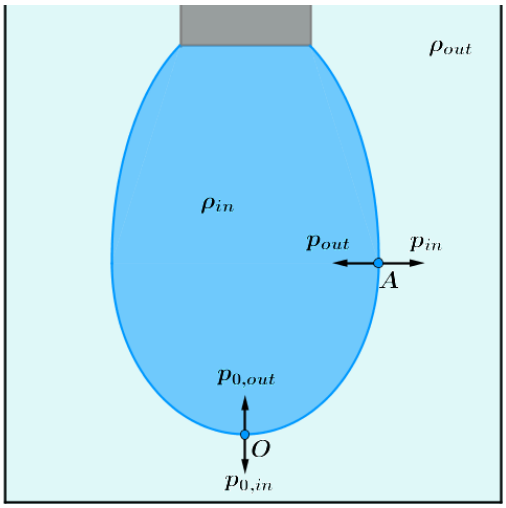

Figure 2.16: Forces acting on the pendant drop

pressure out of the drop and p_{in} is the pressure inside the drop. From (A.5) we have

$$p_{in} = p_{0,in} - \rho_{in} g z,$$
$$p_{out} = p_{0,out} - \rho_{out} g z.$$

Subtracting the latter 2 equations we obtain

$$\underbrace{p_{out} - p_{in}}_{\Delta p} = \underbrace{p_{0,out} - p_{0,in}}_{\Delta p_0} + \underbrace{(\rho_{in} - \rho_{out})}_{\Delta \rho} g z, \tag{2.12}$$

where Δp_0 is the pressure at the apex of the drop. Finally, we must find an expression for p_0. Using the Young-Laplace equation at the apex, we obtain

$$p_0 = \sigma \left(\frac{1}{R_{1,0}} + \frac{1}{R_{2,0}} \right), \tag{2.13}$$

but because the drop is axisymetric, the curvature at the apex can be approximated by a sphere, i.e. $R_{1,0} = R_{2,0} = R_0$. After substituting the latter in (2.13), we obtain

$$p_0 = \frac{2\sigma}{R_0}. \tag{2.14}$$

Combining (2.12) and (2.14), it follows that the equation

$$\Delta p = \Delta p_0 + \Delta \rho g z = \frac{2\sigma}{R_0} + \Delta \rho g z \tag{2.15}$$

holds true. Finally, from (2.11) and (2.12) we obtain

$$\begin{aligned} \frac{dx}{ds} &= \cos\varphi, \\ \frac{dz}{ds} &= \sin\varphi, \\ \frac{d\varphi}{ds} &= \frac{2}{R_0} + \frac{\Delta\rho g z}{\sigma} - \frac{\sin\varphi}{x}. \end{aligned} \tag{2.16}$$

If we introduce the notation $b := \frac{1}{R_0}$ and $c := \dfrac{\Delta\rho g}{\sigma}$, we can rewrite the model for pendant drops in the following form:

$$\begin{aligned} \frac{dx}{ds} &= \cos\varphi, \\ \frac{dz}{ds} &= \sin\varphi, \\ \frac{d\varphi}{ds} &= 2b + cz - \frac{\sin\varphi}{x}. \end{aligned} \tag{2.17}$$

For the initial conditions we take $x(0) = z(0) = \varphi(0) = 0$.

It is obvious that there is a singularity in the third equation when $s = 0$. From the definition of curvature at the apex it follows that $\left.\dfrac{d\varphi}{ds}\right|_{s=0} = b$, where b is the curvature at the apex. We will use this as the definition of the right-hand side of the third equation at $s = 0$.

2.3.3 Derivation of the model for sessile drop

The technology of optical tensiometers for sessile drops is almost the same as the optical tensiometers for pendant drops, described in the Introduction. The only difference is that the tube is coming from the bottom and because of that we must define a different coordinate system as shown in Fig. 2.17. Therefore,

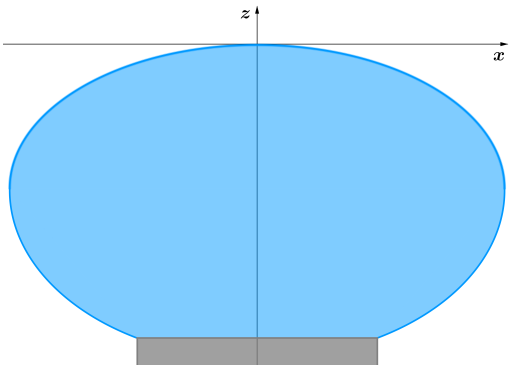

Figure 2.17: Defining a coordinate system in the case of a sessile drop.

we can use the model, derived in the previous subsection.

2.3.4 Derivation of the model for rotational drop

The technology of optical tensiometers for rotating drops is different. A drop is put in a rotating tube.

Figure 2.18: Defining a coordinate system in the case of a rotating drop.

Let us define a coordinate system as shown in Fig. 2.18. Using (2.11) and the pressure in the drop

$$\Delta p = \frac{\omega x^2}{2} + p_{hydr},$$

where p_{hydr} is the hydrostatic pressure, analogously to (2.15) from the latter equation, we obtain

$$\Delta p = \frac{\omega x^2}{2} + \Delta p_0.$$

Because of the technology (the tube is rotating really fast), we can neglect the gravitational force. Therefore, for rotating drops we obtain

$$\begin{aligned} \frac{dx}{ds} &= \cos\varphi, \\ \frac{dz}{ds} &= \sin\varphi, \\ \frac{d\varphi}{ds} &= 2b + dx^2 - \frac{\sin\varphi}{x}, \end{aligned} \tag{2.18}$$

where $b := \frac{1}{R_0}$, $d := \frac{\omega}{2\sigma}$ and R_0 is the radius of curvature at the apex.

2.4 Numerical experiments

For our further research we need to be able to construct a theoretical profile of the drop using system (2.17) or (2.18), assuming that the coefficients b and c (respectively b and d) are known. We shall use the Euler method and the fourth order Runge–Kutta method.

2.4.1 Explicit Euler Method

Let us consider the following autonomous Cauchy problem:

$$\begin{aligned} &\frac{du(t)}{dt} = f(u(t)),\ t \in (t_0, T], \\ &u(t_0) = u_0, \end{aligned} \tag{2.19}$$

where $u : \mathbb{R} \to \mathbb{R}^n,\ f : \mathbb{R}^n \to \mathbb{R}^n$.

Let us introduce the following mesh:

$$\tilde{\omega} := \left\{ t_i = t_0 + i\tau,\ i = \overline{0, n},\ n = \frac{T - t_0}{\tau} \right\}$$

and denote the approximate solution of (2.19) at the point t_i by y_i, for $i = \overline{0, n}$, $y_i \in \mathbb{R}^n$. Using the following approximation of $\frac{du(t)}{dt}$:

$$\frac{du}{dt} = \frac{u(t + \tau) - u(t)}{\tau} + O(\tau),$$

we find the relation

$$\frac{y_{i+1} - y_i}{\tau} = f(y_i) \tag{2.20}$$

between the values of the approximate solution at two consecutive points. The geometric interpretation of this method is illustrated in Fig. 2.19 and given in the following algorithm.

1. Let us start from the initial conditions $y_0 = u_0$.
2. We assume that we have found the points $(t_i, y_i),\ i = \overline{0, k}$ for some $k < n$.
3. Using (2.20), we draw the tangent $l(t)$ to the graph at the point (t_k, y_k) and we approximate the value of $u(t_{k+1})$ with $y_{k+1} = l(t_{k+1})$.

Using this method, we construct the following numerical schemes that give us the approximate solutions of (2.17) and (2.18).

- For pendant drop:

$$\begin{aligned} x_{i+1} &= x_i + \tau \cos\varphi_i, \\ z_{i+1} &= z_i + \tau \sin\varphi_i, \\ \varphi_{i+1} &= \varphi_i + \tau \left(2b + cz_i - \frac{\sin\varphi_i}{x_i} \right). \end{aligned} \tag{2.21}$$

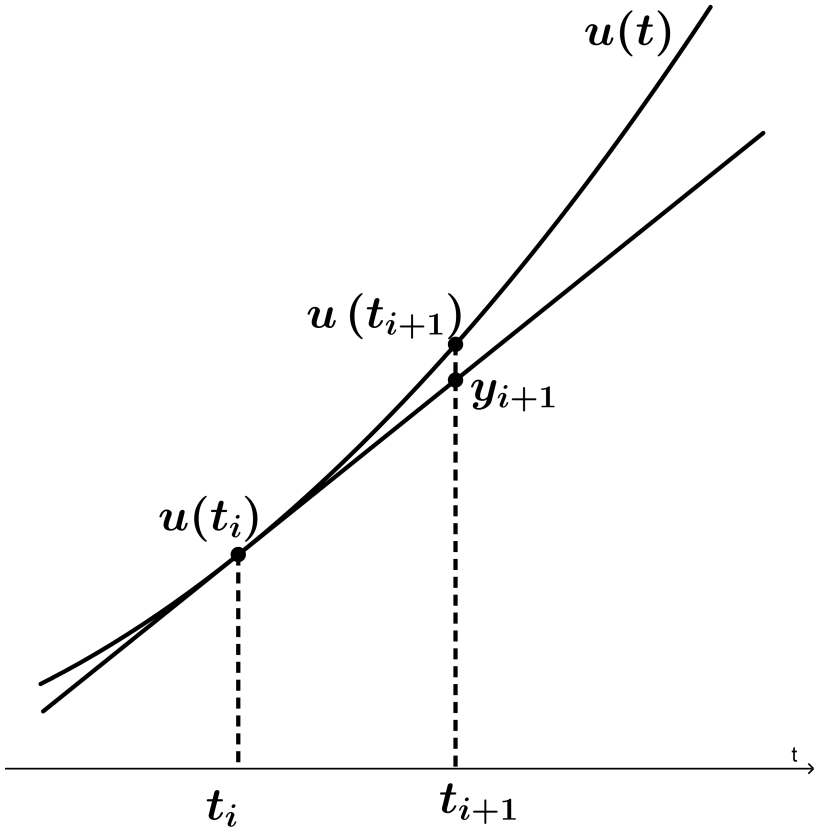

Figure 2.19: Geometric interpretation of the Euler method.

- For rotating drop:

$$\begin{aligned} x_{i+1} &= x_i + \tau \cos\varphi_i, \\ z_{i+1} &= z_i + \tau \sin\varphi_i, \\ \varphi_{i+1} &= \varphi_i + \tau \left(2b + dx_i^2 - \frac{\sin\varphi_i}{x_i} \right). \end{aligned} \tag{2.22}$$

We have tested the Euler method by studying the results it gives for drop's profiles with known values of the parameters. As shown in Fig. 2.20 and Fig. 2.22, it recovers the known shapes with very good accuracy. In Fig. 2.21 and Fig. 2.23 drop's profiles with changed parameters are shown. Obviously, in order to obtain the correct result, we need to compute the model parameters with sufficiently good accuracy.

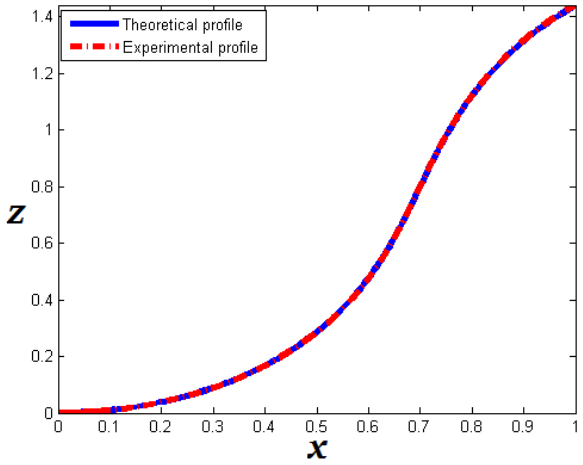

Figure 2.20: Experimental and theoretical profiles of a pendant drop. The exact solution corresponds to parameters $b = 1.84365781711$ and $c = -2.9$.

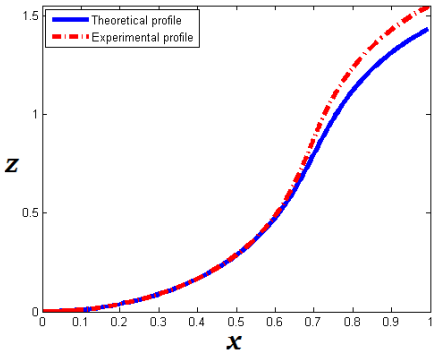

(a) $b = 1.84365781711$, $c = -2.7$

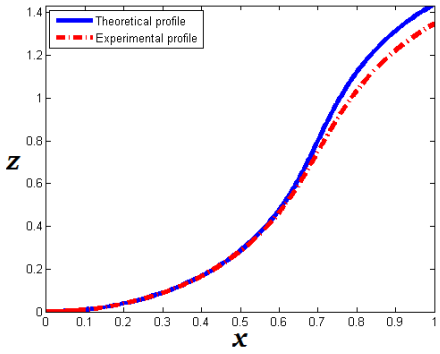

(b) $b = 1.84365781711$, $c = -3.1$

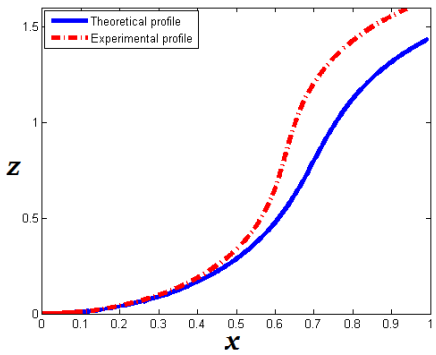

(c) $b = 2$, $c = -2.9$

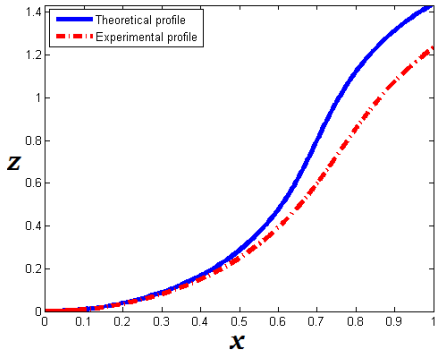

(d) $b = 1.7$, $c = -2.9$

Figure 2.21: Sensitivity of the solutions with respect to the model parameters. The exact solution corresponds to the parameters $b = 1.84365781711$, and $c = -2.9$

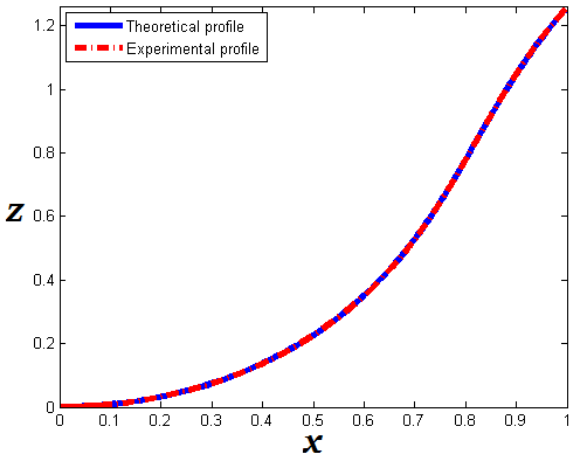

Figure 2.22: Experimental and theoretical profiles, obtained with the Euler method, for a pendant drop. The exact solution corresponds to parameters $b = 1.57480314961$ and $c = -2.3$.

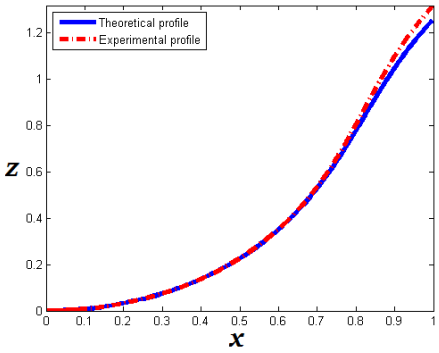

(a) $b = 1.57480314961$, $c = -2.3$

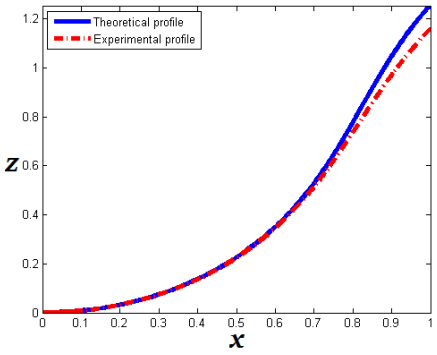

(b) $b = 1.57480314961$, $c = -2.6$

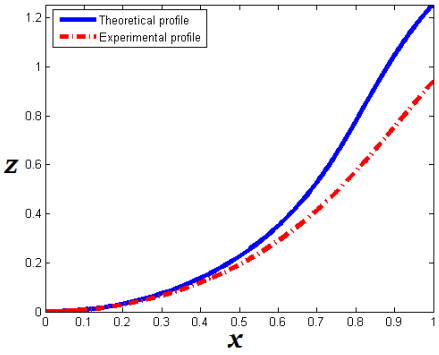

(c) $b = 1.4$, $c = -2.3$

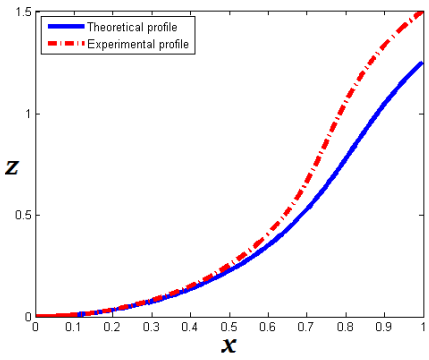

(d) $b = 1.7$, $c = -2.3$

Figure 2.23: Sensitivity of the solutions with respect to the model parameters. The exact solution corresponds to the parameters $b = 1.84365781711$, and $c = -2.9$.

2.4.2 Fourth order explicit Runge-Kutta method

The family of explicit Runge–Kutta methods are methods used for solving the Cauchy problem (2.19). The s-stage explicit Runge-Kutta method is given by the formula

$$\frac{y_{n+1}-y_n}{h} = \frac{1}{h}\sum_{i=1}^{s} b_i k_i, \tag{2.23}$$

where k_i are given by

$$\begin{aligned}
k_1 &= hf(t_n, y_n),\\
k_2 &= hf(t_n + \alpha_2 h, y_n + \beta_{21} k_1),\\
k_3 &= hf(t_n + \alpha_3 h, y_n + \beta_{31} k_1 + \beta_{32} k_2),\\
&\dots\\
k_s &= hf(t_n + \alpha_s h, y_n + \beta_{s1} k_1 + \beta_{s2} k_2 + \dots + \beta_{s,s-1} k_{s-1}).
\end{aligned}$$

To specify a given method, it is enough to provide s (the number of stages), α_k, β_{km}, and b_k. The parameters can be found so that they minimize the local truncation error. We will use the 4-stage Runge-Kutta, i.e.

$$\frac{y_{n+1}-y_n}{h} = \frac{1}{h}\sum_{i=1}^{4} b_i k_i,$$

where

$$\begin{aligned}
k_1 &= hf(t_n, y_n),\\
k_2 &= hf(t_n + \alpha_2 h, y_n + \beta_{21} k_1),\\
k_3 &= hf(t_n + \alpha_3 h, y_n + \beta_{31} k_1 + \beta_{32} k_2),\\
k_4 &= hf(t_n + \alpha_4 h, y_n + \beta_{41} k_1 + \beta_{42} k_2 + \beta_{43} k_3).
\end{aligned}$$

It can be shown that the local truncation error of the 4-stage Runge-Kutta method is $O(h^4)$ and from this computations we can obtain the following numerical scheme:

$$y_{n+1} = y_n + \frac{h}{6}(k_1 + 2k_2 + 2k_3 + k_4),$$

where

$$\begin{aligned}
k_1 &= hf(t_n, y_n),\\
k_2 &= hf\left(t_n + \frac{h}{2}, y_n + \frac{k_1}{2}\right),\\
k_3 &= hf\left(t_n + \frac{h}{2}, y_n + \frac{k_2}{2}\right),\\
k_4 &= hf(t_n + h, y_n + k_3).
\end{aligned}$$

We will solve the system (2.17) or (2.18). For this purpose we will solve simultaneously all equations using the Runge–Kutta method. Let us introduce

the notation $u := (x, z, \varphi)^T$ and $f := (f_1, f_2, f_3)^T$, where f_1, f_2, and f_3 are the right-hand sides of the model (2.17) or (2.18).

In order to test our numerical scheme, we shall compare the obtained results with known experimental profiles for given values of the model parameters.

As can be seen from Fig. 2.24 and Fig. 2.25, the method gives satisfactory results.

In Fig. 2.26 we study the sensitivity of the solution with respect to the model parameters. Perturbations in both parameters can lead to changes in the solutions.

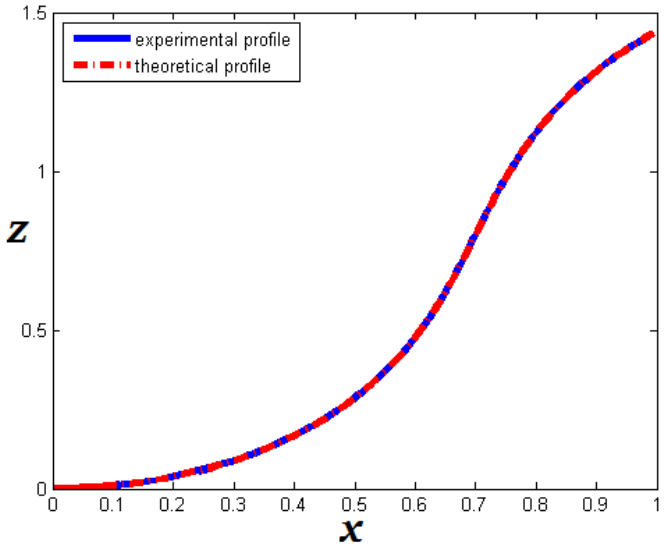

Figure 2.24: Experimental and theoretical profiles of a pendant drop. The exact solution corresponds to parameters $b = 1.84365781711$ and $c = -2.9$.

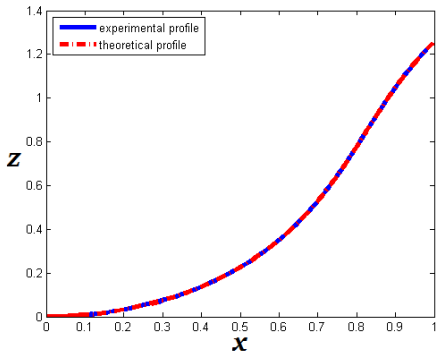

(a) $b = 1.57480314961$ and $c = -2.3$ for drop 2

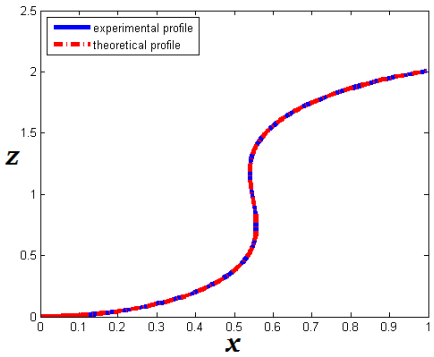

(b) $b = 2.06440957886$, $c = -2.4$ for drop 3

Figure 2.25: Experimental and theoretical profiles, obtained with the Runge–Kutta method, of pendant drops.

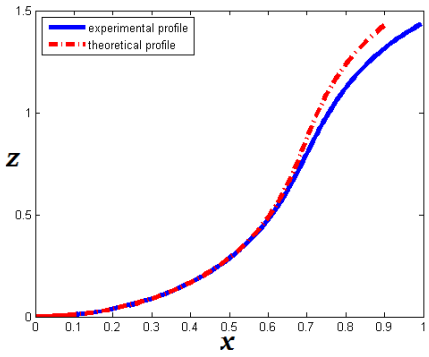

(a) $b = 1.84365781711$, $c = -2.7$

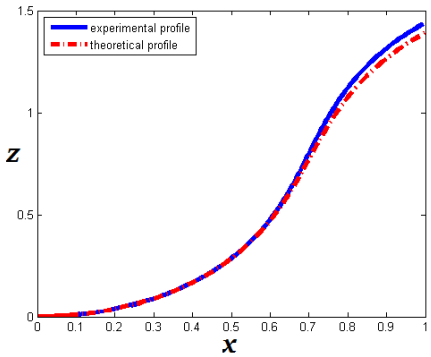

(b) $b = 1.84365781711$, $c = -3$

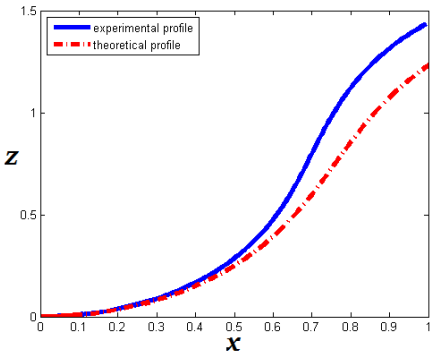

(c) $b = 1.7$, $c = -2.9$

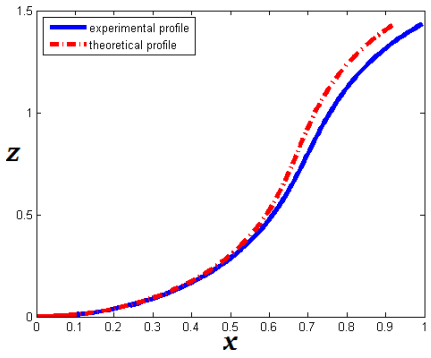

(d) $b = 1.9$, $c = -2.9$

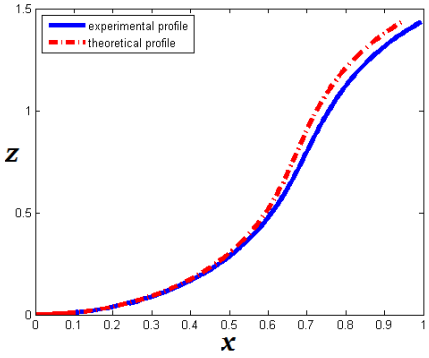

(e) $b = 1.9$, $c = -2.95$

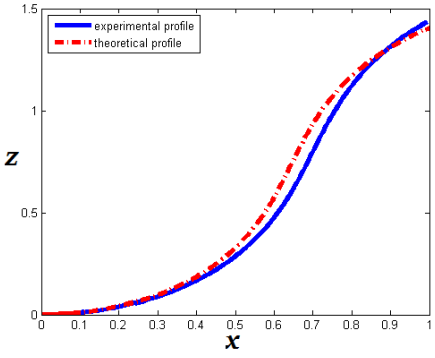

(f) $b = 2$, $c = -3.4$

Figure 2.26: Sensitivity of the solutions with respect to the model parameters. The exact solution corresponds to the parameters $b = 1.84365781711$, and $c = -2.9$.

2.5 Parametric Identification

The main purpose of this paper is to find a way to determine the surface tension of a liquid material by analyzing an image of a drop of this material. We shall accomplish this in two different ways, by using two distinct optimization algorithms — the Deepest descent and the Gauss-Newton methods. For both the algorithms we use the same objective function that we call the error function and describe it in the paragraph below.

2.5.1 Error function

First, we have to define a function that for any given values of the parameters b and c will give us a numerical representation of the "distance" between the theoretical and the experimental profiles. We shall call this function the error function ($Err(b, c)$) and will define it in the following way (see Fig. 2.27).

1. Let $\{(x_i, z_i)\}_{i=1}^{n_1}$ be the cloud of points derived from the experimental data and $\{(\tilde{x}_i, \tilde{z}_i)\}_{i=1}^{n_2}$ be the cloud of points acquired from the numerical solution of the ODE system, for given parameters b and c.

2. For every point in the theoretical profile, $(\tilde{x}_i, \tilde{z}_i),\ i = \overline{1, n_2}$, let us find the following two points (see Fig. 2.27):

$$\begin{aligned}(x_{i_1}, z_{i_1}) :&\ x_{i_1} = \max_{x_i \le \tilde{x}_i} x_i,\\ (x_{i_2}, z_{i_2}) :&\ x_{i_2} = \min_{x_i \ge \tilde{x}_i} x_i.\end{aligned}$$

   We ignore all the points $(\tilde{x}_i, \tilde{z}_i)$ for which the following inequalities hold:

$$\begin{aligned}\tilde{x}_i &< \min_{0 \le i \le n_1} x_i,\\ \tilde{x}_i &> \max_{0 \le i \le n_1} x_i.\end{aligned}$$

3. Now let us construct a line $l_i : (x_{i_1}, z_{i_1}),\ (x_{i_2}, z_{i_2}) \in l_i$. We shall denote the distance between the point $(\tilde{x}_i, \tilde{z}_i)$ and the line l_i by d_i,

$$d_i := dist((\tilde{x}_i, \tilde{z}_i), l_i).$$

   If for some point $(\tilde{x}_k, \tilde{z}_k)$

$$\tilde{x}_k = \max_{x_i \le \tilde{x}_i} x_i = \min_{x_i \ge \tilde{x}_i} x_i = x_{i_k},$$

   then $d_i := dist((\tilde{x}_k, \tilde{z}_k), (x_{i_k}, z_{i_k}))$.

4. We define the error function $Err : \mathbb{R}^2 \to \mathbb{R}$ to be

$$Err(b, c) = \sum_{i=1}^{n_2} d_i^2.$$

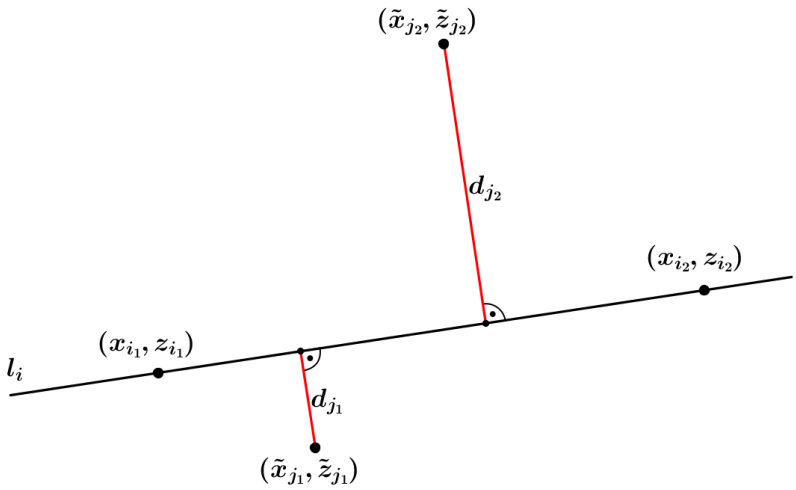

Figure 2.27: Definition of the error function.

2.5.2 Initial guess

The optimization methods we use depend strongly on having an accurate initial guess for the parameters b and c. This we shall obtain from the experimental data. From the third equation in (2.21) or (2.22) we obtain the system

$$A.X = B, \tag{2.24}$$

where:

- for pendant drop:

$$A = \begin{bmatrix} 2\tau & \tau z_1 \\ 2\tau & \tau z_2 \\ \vdots & \vdots \\ 2\tau & \tau z_{n-1} \end{bmatrix}, \; X = \begin{bmatrix} b \\ c \end{bmatrix}, \; B = \begin{bmatrix} \varphi_2 - \varphi_1 + \tau \frac{\sin \varphi_1}{x_1} \\ \vdots \\ \varphi_n - \varphi_{n-1} + \tau \frac{\sin \varphi_{n-1}}{x_{n-1}} \end{bmatrix};$$

- for rotating drop:

$$A = \begin{bmatrix} 2\tau & \tau x_1^2 \\ 2\tau & \tau x_2^2 \\ \vdots & \vdots \\ 2\tau & \tau x_{n-1}^2 \end{bmatrix}, \; X = \begin{bmatrix} b \\ d \end{bmatrix}, \; B = \begin{bmatrix} \varphi_2 - \varphi_1 + \tau \frac{\sin \varphi_1}{x_1} \\ \vdots \\ \varphi_n - \varphi_{n-1} + \tau \frac{\sin \varphi_{n-1}}{x_{n-1}} \end{bmatrix}.$$

Now, let us substitute x_i, z_i in the latter with our experimental data. Because our raw data consists only of points with coordinates (x, z) we use the following formula to calculate the values of the angle φ at every point from our data:

$$\varphi_i = \arctan \frac{z_i - z_{i-1}}{x_i - x_{i-1}}, \;\; i = \overline{1, n_1}.$$

The Euler method states that (2.24) will hold approximately, so by solving it we obtain an initial estimation of the model parameters.

2.5.3 Deepest descent method

The idea of the Deepest descent method is, starting from some initial guess $v_1 = (b_{initial}, c_{initial})$ for the model's parameters, to obtain a sequence of consecutive estimations $\{v_n\}_{n=1}^{k}$, going in the direction of the negative gradient vector. The direction of the negative gradient vector is toward the closest local minimum. Because our function $Err(b, c)$ is non-constant and non-negative, the point (b_{real}, c_{real}), where b_{real} and c_{real} are the actual values of the parameters b and c, is a local (and overall) minimum. Due to this fact, if we start with a sufficiently accurate initial guess for b and c, the negative gradient vector will point towards the real values.

We implement this idea in the following algorithm:

1. We begin with the initial guess $v_1 = (b_{initial}, c_{initial})$.

2. For $k = 1, 2, \ldots$:

   (a) we obtain an approximation v_k with the formula

   $$v_k = v_{k-1} - \alpha \nabla Err(v_k),$$

   where α is a number for which the following inequality holds:

   $$Err(v_k) < Err(v_{k-1}).$$

   (b) If

   $$Err(v_k) < \epsilon$$

   for some error tolerance, ϵ, we stop the algorithm and take v_k to be the approximation of the optimal solution.

Now, let us see what results our optimization methods yields. For several sets of experimental data we were able to approximate the values of b and c. Using the Euler method, we drew the theoretical profile with the estimated values of b and c and compared it to the experimental profile, see Fig. 2.28 and Fig. 2.29.

As we can see, if we have a good initial guess the method converges to appropriate values for b and c.

2.5.4 Gauss–Newton method

The Gauss-Newton method is an optimization algorithm. Suppose we are given a set of data points $\{(x_i, y_i)\}_{i=1}^{n}$ (i.e., the experimental profile). We want to obtain b and c, so that $Err(b, c)$ is minimized. In order to do so we set

$$g(b, c) := \nabla Err = \begin{bmatrix} \dfrac{\partial Err(b,c)}{\partial b} \\ \dfrac{\partial Err(b,c)}{\partial c} \end{bmatrix} = 0.$$

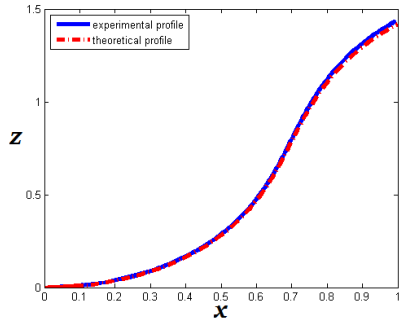

(a) The final values of the parameters b=1.8451 and c=-2.902, using the Euler method.

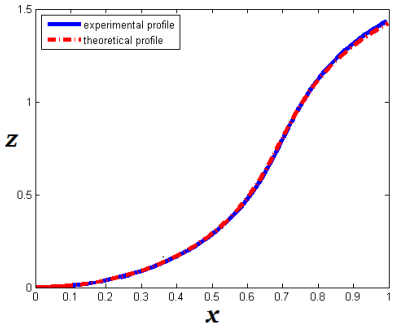

(b) The final values of the parameters b=1.8602 and c=-2.9782, using the Runge–Kutta method.

Figure 2.28: Results of the parametric identification for a pendant drop, using the Deepest Descent method.

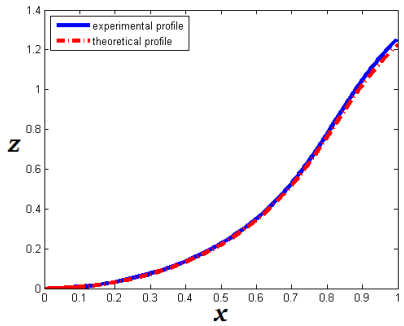

(a) The final values of the parameters b=1.5755 and c=-2.4861, using the Euler method.

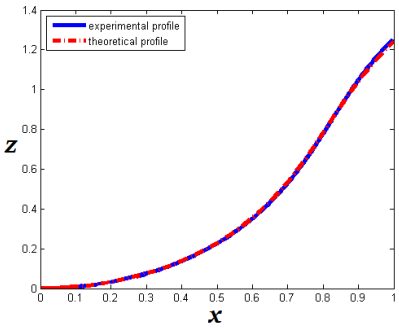

(b) The final values of the parameters b=1.5898 and c=-2.4851, using the Runge–Kutta method.

Figure 2.29: Results of the parametric identification for a pendant drop, using the Deepest Descent method.

We represent $g(b,c)$ as Taylor series and obtain consecutively

$$0 = g(b_{i+1}, c_{i+1}) = g(b_i + \Delta b, c_i + \Delta c) \approx g(b_i, c_i) + \nabla g(b_i, c_i) \cdot \begin{bmatrix} \Delta b \\ \Delta c \end{bmatrix},$$

$$\begin{bmatrix} \Delta b \\ \Delta c \end{bmatrix} \approx -(\nabla g(b_i, c_i))^{-1} g(b_i, c_i) = -H^{-1} \nabla Err(b_i, c_i),$$

$$\begin{bmatrix} b_{i+1} \\ c_{i+1} \end{bmatrix} \approx \begin{bmatrix} b_i \\ c_i \end{bmatrix} - H^{-1} \nabla Err(b_i, c_i)$$

where H is the Hessian of the function $Err(b,c)$. We implement this idea in the following algorithm.

1. We begin with the initial guess $k_1 = (b_{initial}, c_{initial})$.
2. For $i = 1, 2, \ldots$:

(a) we obtain an approximation k_{i+1} with the formula

$$\begin{bmatrix} b_{i+1} \\ c_{i+1} \end{bmatrix} \approx \begin{bmatrix} b_i \\ c_i \end{bmatrix} - H^{-1}\nabla Err(b_i, c_i), \tag{2.25}$$

where we approximate the first partial derivatives in the gradient, using first order forward divided differences and the derivatives in the Hessian, using second order central divided differences.

(b) If

$$Err(k_{i+1}) < \varepsilon$$

for some error tolerance, ε, we stop the algorithm and take k_{i+1} to be the approximation of the optimal solution.

Using the Gauss-Newton method and refined set of points, originating from the experimental data, we obtain the results shown in Fig. 2.30 and Fig. 2.31. As we can see, the Gauss–Newton method gives satisfactory results for those two drops. For drops, that have an inflection point, however, the results given

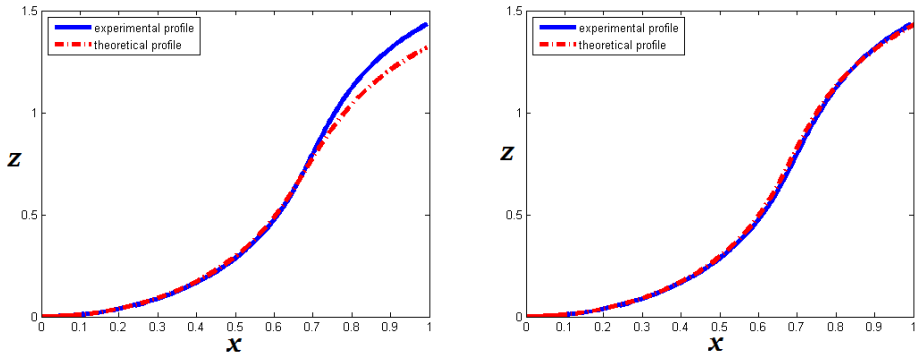

(a) The final values of the parameters b=1.8936 and c=-3.3030 using the Euler method.

(b) The final values of the parameters b=1.8778 and c=-3.0191 using the Runge–Kutta method.

Figure 2.30: Results of the parametric identification for a pendant drop, using the Deepest Descent method.

by the algorithm do not seem to be good. We could argue that the definition of the error function is not adequate for this case and, hence, further improvements should be made.

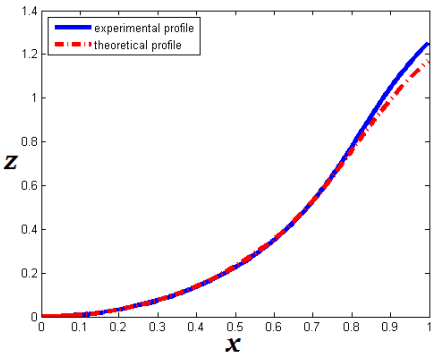

(a) The final values of the parameters b=1.6079 and c=-2.5978, using the Euler method.

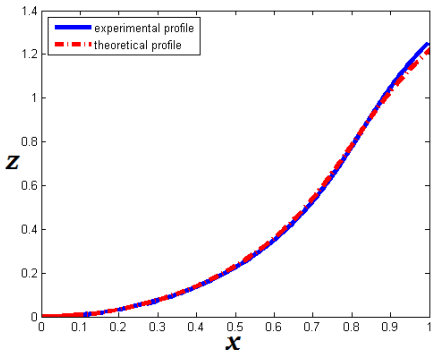

(b) The final values of the parameters b=1.6079 and c=-2.5978, using the Runge–Kutta method.

Figure 2.31: Results of the parametric identification for pendant drops, having no inflection points, using the Gauss-Newton method.

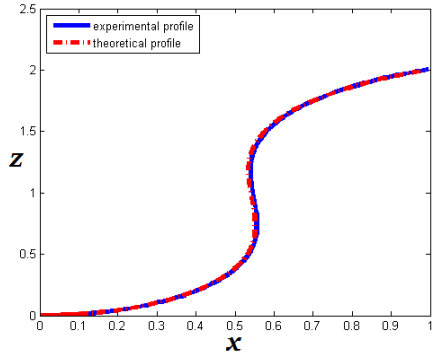

(a) The initial values of the parameters b=2.0793 and c=-2.4246.

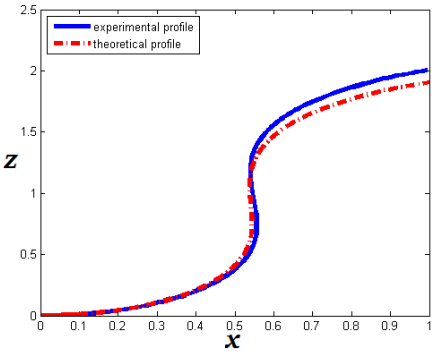

(b) The final values of the parameters b=2.1336 and c=-2.6568.

Figure 2.32: Results of the parametric identification for a pendant drop, having an inflection point, using the Gauss-Newton method.

2.6 Conclusion

We have studied an applied problem of estimating the surface tension of a fluid by estimating the parameters in a model, describing the shape of a drop of the fluid.

The optimization algorithms used in parametric identification algorithms are usually iterative and need a good initial guess. We have proposed an algorithm for the initial estimation that to the best of our knowledge is new and (as the numerical experiments showed) gives very satisfactory results.

In order to have good computational times we have tried comparatively low-order methods for solving the three-dimensional ODE system that describes the drops' profiles. Both the Euler method and the fourth order Runge-Kutta method are sufficient for recovering the drops' profiles in the cases of only gravitational forces or only centrifugal forces acting on the drop.

The Gauss–Newton and the Deepest descent methods were used for minimizing the error function. In the case of drops' profiles having no inflection points both algorithms succeed in finding the correct values of the model parameters provided initial guess by our method. As the numerical experiments showed, the error definition is not adequate in cases when inflection points exist. Thus, further improvement is needed in this direction.

Appendix A

Pressure. Interfacial tension.

Pressure is defined as force per unit area, $p = \frac{F}{A}$, where F is the force and A is the area, on which the force is applied. The pressure is normal to the surface on which it is applied.
Here, we derive the Pascal's law, the formula for the hydrostatic pressure and prove that the hydrostatic pressure depends only on the depth of the container and the density of the liquid.

A.1 Pascal's law for pressure at a point

The Pascal's law states that the pressure at a point is the same in all directions.
Derivation:
Let us consider an infinitesimally small element $ABCDEF$ of a static fluid with triangular prism form, which contains a point P. Let p_x, p_y and p_s be the pressures acting on the three faces of the prism as shown at Fig. A.1.

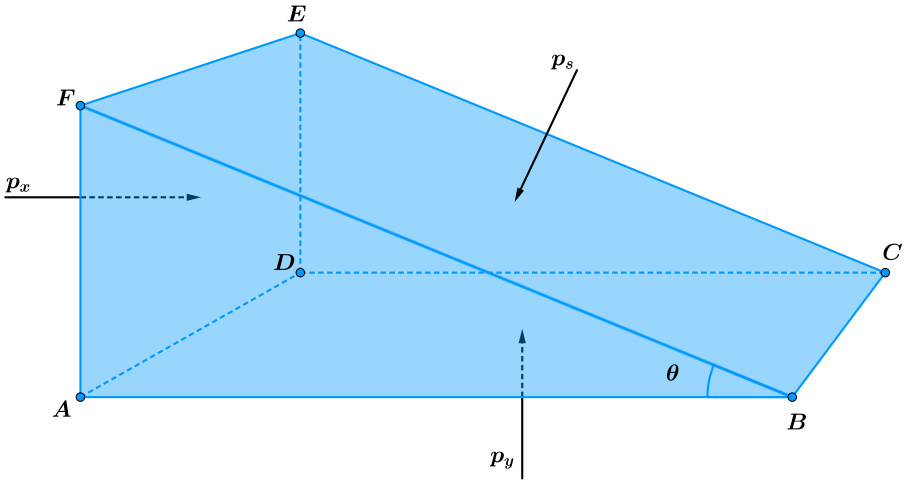

Figure A.1: p_x acts perpendicular to the face $ADEF$, p_y acts perpendicular to the face $ABCD$, p_s acts perpendicular to the face $BCEF$

The fluid is static, thus, the sum of all forces that act on the element is equal to 0. They are

$$\begin{aligned} F_y &= p_y S_{ABCD} = p_y \cdot AB \cdot BC, \\ F_x &= p_x S_{ADEF} = p_x \cdot AD \cdot AF = p_x \cdot BC \cdot AF, \\ F_s &= p_s S_{BCEF} = p_s \cdot BC \cdot BF. \end{aligned} \tag{A.1}$$

Summing the forces in the x-direction, we obtain

$$F_x = F_s \sin\theta,$$

where θ is the angle between AB and BF. Substituting (A.1) into the latter, it follows that

$$\begin{aligned} p_x \cdot BC \cdot AF = p_s \cdot BC \cdot BF \sin\theta = p_s \cdot BC \cdot BF \cdot \frac{AF}{BF}, \\ p_x = p_s. \end{aligned}$$

Summing the forces in the y-direction, we have

$$F_y = F_s \sin\theta + weight.$$

Contracting the prism to a point, and, thus, neglecting the weight of the fluid, we obtain consecutively

$$\begin{aligned} F_y &= F_s \sin\theta, \\ p_y \cdot AB \cdot BC = p_s \cdot BC \cdot BF \cos\theta &= p_s \cdot BC \cdot BF \cdot \frac{AB}{BF}, \\ p_y &= p_s. \end{aligned}$$

Thus, we proved that $p_x = p_y = p_s$ in a point, where p_s is the pressure at an arbitrary angle, θ, from the x-axis, i.e. the pressure is the same in all directions.

A.2 Hydrostatic pressure

Here, we derive a formula for the hydrostatic pressure at depth H in an arbitrarily shaped vessel. First, we derive the model for a tank having rectangular parallelepiped shape. Then, we consecutively show that the pressure at equal depths is the same in cylinder and in curved shaped tank.

A.2.1 Hydrostatic pressure in rectangular parallelepipeds

Let us consider a rectangular parallelepiped, containing liquid and let it be subjected only to gravitational forces. Then, two kinds of pressure are induced in it — hydrostatic and atmospheric (see Fig. A.2). The hydrostatic pressure at a point is the pressure due to the weight of the liquid that is above the horizontal plain, containing the point in consideration. The atmospheric pressure is exerted

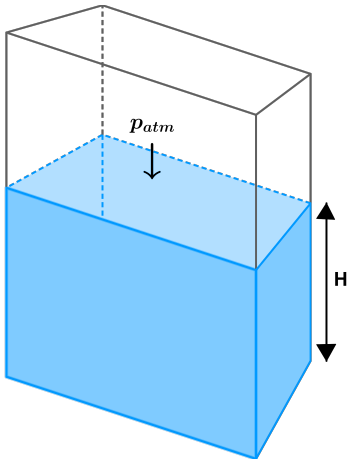

Figure A.2: Hydrostatic pressure in a rectangular parallelepiped, in which the level of water is H and p_{atm} is the atmospheric pressure that acts on it.

by the weight of the air on the surface.
Thus, the pressure at depth H at the water tank has two contributions, i.e.

$$p = p_{atm} + p_{hydrost}, \tag{A.2}$$

where p_{atm} and $p_{hydrost}$ are the corresponding atmospheric and hydrostatic pressures. For the hydrostatic contribution, taking into account that it is induced by the weight force, we have

$$p_{hydrost} = \frac{G}{A} = \frac{mg}{A} = \frac{V\rho g}{A} = H\rho g, \tag{A.3}$$

where m is the mass of water, V is the volume of the drop, ρ is the density of the fluid, A is the cross-sectional area of the tank and H is the height of the water. Here, we used the fact that the tank is a rectangular parallelepiped and, thus, $V = AH$ holds. Substituting (A.3) in (A.2), we finally obtain

$$p = p_{atm} + \rho g H. \tag{A.4}$$

Remark: If we want to express the pressure on a plain P_1 at depth $h + H$ with respect to the pressure on the plain P_2 at depth h (Fig. A.3), it is obvious that

$$p_1 = p_{atm} + \rho g(H + h),$$
$$p_2 = p_{atm} + \rho g h.$$

Then, we subtract the second equation from the first one and obtain

$$p_1 = p_2 + \rho g H. \tag{A.5}$$

A.2.2 Equality of pressures at the same depth

Now, we shall prove that formula (A.5) can be used for tanks with arbitrary shapes and the pressure depends only on the depth.

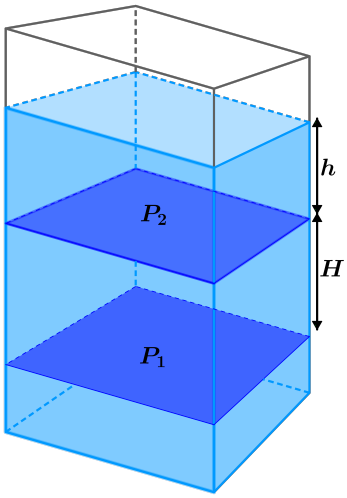

Figure A.3: Hydrostatic pressure in a rectangular parallelepiped tank, in which the level of water in plain P_1 is $H + h$ and in plain P_2 is h.

First, we will show that the hydrostatic pressure in horizontal direction is a constant in any continuous fluid. This is obvious, when we are talking about the pressure in a rectangular parallelepiped, because of formula (A.4). But this is true also for all forms of containers. Let us consider a cylinder, full of fluid.

Figure A.4: Hydrostatic pressure in an infinitesimally small cylinder.

The fluid is static, thus, the sum of the forces is 0. The forces are

$$F_a = p_a A,$$
$$F_b = p_b A$$

and, thus,

$$p_a = p_b,$$

where p_a is the pressure on the left side, p_b – pressure on the right side and A is the cross-sectional area of the cylinder. If the cylinder is infinitesimally small, then the pressure in two points at the same level is constant (see Fig. A.4).

A.2.3 Hydrostatic pressure in communicating vessels

Let A and B are arbitrary points at depth h_1 at communicating vessels (see Fig. A.5). We shall prove that the pressure in the points A and B is the same. Using (A.5), we obtain

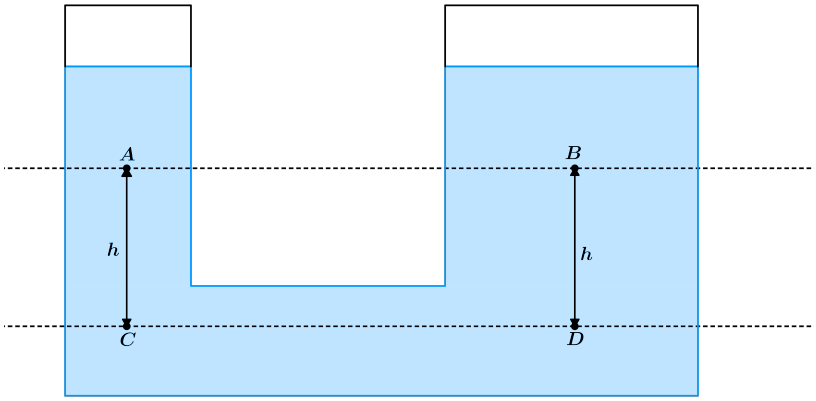

Figure A.5: Hydrostatic pressure in communicating vessels.

$$p_c = p_a + \rho g h,$$
$$p_d = p_b + \rho g h.$$

Taking into account that $p_c = p_d$, it follows that $p_a = p_b$ holds.

A.2.4 Hydrostatic pressure in arbitrarily shaped tanks

Finally, let us consider an arbitrary shape, see Fig. A.6. We want to find the

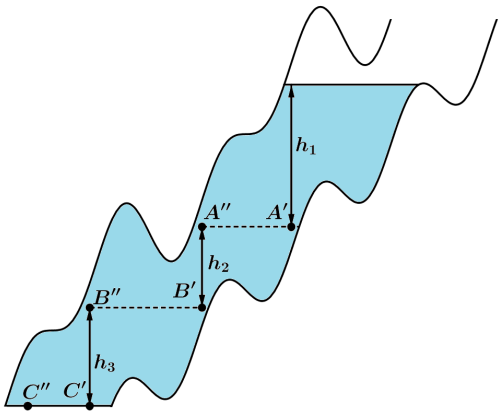

Figure A.6: Hydrostatic pressure in an arbitrary shape.

hydrostatic pressure at the point C''. First, we can find the pressure at the point

A' : $p_{A'} = \rho g h_1$. The pressure at A'' is the same as the pressure at A'. Pressure at B'' is

$$p_{B''} = p_{B'} = P''_A + \rho g h_2 = \rho g(h_1 + h_2).$$

Finally, at C'' we have

$$p_{C''} = p_{C'} = P''_B + \rho g h_3 = \rho g(h_1 + h_2 + h_3).$$

This reasoning can obviously be applied to an arbitrary shape and, hence, **hydrostatic pressure depends only on density of the liquid, gravity force and depth**. It does not depend on the volume of the liquid or the shape of the tank that the liquid is in.

A.3 Surface tension

Surface tension is an effect within the surface of a liquid that causes it to behave as an elastic membrane.

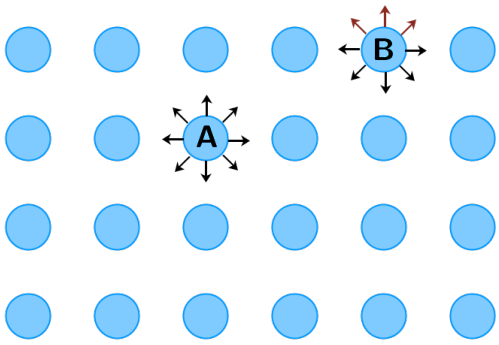

Figure A.7: Forces acting on the particles in a fluid

Let us consider static fluid and a particle A inside the fluid. All the cohesive forces [1], acting on that particle, cancel out. On the other hand, the forces that act on the particle B (on the surface of the liquid) do not cancel out, because on the surface there are adhesive forces[2] between the molecule and for example the air (see Fig. A.7). The magnitude of the adhesive forces is smaller than the magnitude of the cohesive, thus, the resultant force points to the liquid. Because of this the bubbles have spherical form.

The surface tension is measured as the energy required to increase the surface area of a liquid by a unit of area or force per unit length.

[1] Cohesive forces are the intermolecular forces, which are the reason why the molecules in liquids stick together. These forces exist between molecules of the same substance.

[2] Adhesive forces are the attractive forces between two or more different molecules.

Appendix B

Curvature

B.1 Plain Curves

First, we define the curvature of a plain curve. In order to do so, we shall examine the behaviour of the tangent and the normal vectors to the curve. Let us consider a plain parametric curve $r(u)$. Let $A = r(u)$ and $B = r(u + \Delta u)$ be two points from the curve and O be the origin of the coordinate system. The vector $\overrightarrow{AB}$ is, thus,

$$\overrightarrow{AB} = \overrightarrow{OB} - \overrightarrow{OA} = r(u + \Delta u) - r(u),$$

see Fig. B.1. If A tends to B ($\Delta u \to 0$), then the vector $\overrightarrow{AB}$ tends to the tangent vector $\lim_{\Delta u \to 0} [r(u + \Delta u) - r(u)]$. Let us introduce the notation

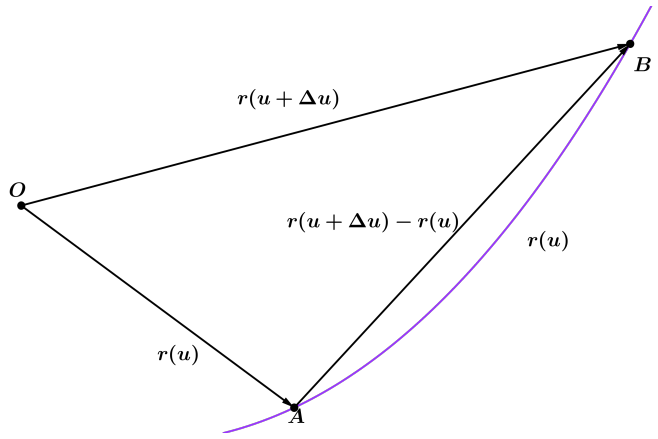

Figure B.1: The vector $r(u+\Delta u)-r(u)$ tends to the tangent vector as $\Delta u \to 0$.

$$\frac{dr}{du} := \lim_{\Delta u \to 0} \frac{r(u + \Delta u) - r(u)}{\Delta u}.$$

Then, we can say that $\frac{dr}{du}$ is a tangent vector and the unit tangent vector t is

$$t = \frac{\frac{dr}{du}}{\left|\frac{dr}{du}\right|}, \tag{B.1}$$

where

$$\left|\frac{dr}{du}\right| = \lim_{\Delta u \to 0} \frac{|r(u+\Delta u) - r(u)|}{\Delta u}.$$

If we approximate the length of the segment AB (i.e., $|r(u+\Delta u) - r(u)|$) with the length of $\overset{\frown}{AB}$ (let us denote it by Δs), we obtain

$$\left|\frac{dr}{du}\right| = \lim_{\Delta u \to 0} \frac{\Delta s}{\Delta u} = \frac{ds}{du}. \tag{B.2}$$

From (B.1) and (B.2) we obtain

$$t = \frac{dr}{ds}.$$

Therefore, the unit tangent vector is the derivative of the curve with respect to the arc length. If $r(s)$ is the curve parameterized by the arc length, then we define

$$\frac{d^2r}{ds^2} = \lim_{\Delta s \to 0} \frac{r'(s+\Delta s) - r'(s)}{\Delta s},$$

where $'$ denotes $\frac{d}{ds}$. It is known that $r'(s+\Delta s)$, $r'(s)$ are tangent vectors (see Fig. B.2). When A tends to B, $r'(s)$ tends to $r'(s+\Delta s)$ and the vector $r'(s+$

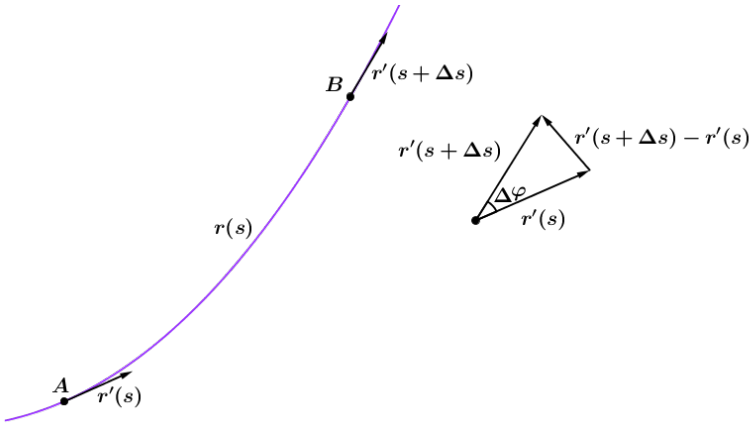

Figure B.2: The vector $r'(s+\Delta s) - r'(s)$ tends to the normal vector as $\Delta s \to 0$.

$\Delta s) - r'(s)$ tends to the vector perpendicular to the tangent vector. The unit vector n is defined as follows

$$n = \frac{r''(s)}{|r''(s)|} = \frac{t'}{k}, \tag{B.3}$$

where k is called curvature at a point. We can define k as

$$k = |r''(s)| = \lim_{\Delta s \to 0} \frac{|r'(s+\Delta s) - r'(s)|}{\Delta s} = \lim_{\Delta s \to 0} \frac{|\sin \Delta\varphi|}{\Delta s}.$$

Taking into account that $\Delta s \to 0$, it follows that $\Delta\varphi \to 0$, then $\sin|\Delta\varphi| \approx |\Delta\varphi|$ holds true and

$$k = |r''(s)| = \lim_{\Delta s \to 0} \frac{\Delta\varphi}{\Delta s} =: \frac{d\varphi}{ds}.$$

Curvatures of lines and circles

Let t_A and t_B denote the tangents to the curve at two different points A and B, see Fig. B.3, and φ_A and φ_B are the corresponding angles between the tangents and the x-axis. For a line, the curvature at any point is 0, because

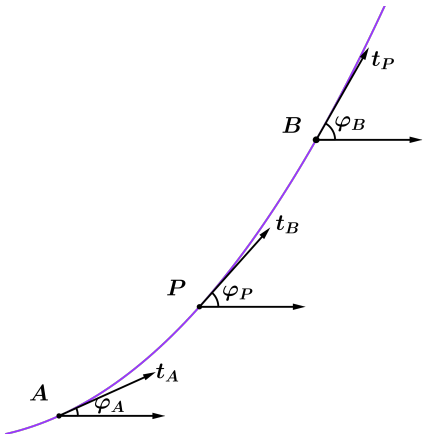

Figure B.3: The curvature is defined as $k = \frac{d\varphi}{ds}$.

$$k = \lim_{\Delta s \to 0} \frac{\varphi_B - \varphi_A}{\Delta s} = \lim_{\Delta s \to 0} \frac{\varphi_A - \varphi_A}{\Delta s} = 0.$$

For a circle, we have

$$k = \lim_{\Delta s \to 0} \frac{\varphi_B - \varphi_A}{\Delta s}.$$

Using the notation from Fig. B.4, $\angle APB = \varphi$ and $m \parallel l$, then $\angle PBQ = \varphi$. Thus, the angle between m and n is equal to $\frac{\pi}{2} + \varphi$. Therefore, the following equality holds:

$$k = \lim_{\Delta s \to 0} \frac{\varphi_B - \varphi_A}{\Delta s} = \lim_{\Delta s \to 0} \frac{\frac{\pi}{2} + \varphi - \frac{\pi}{2}}{\Delta s} = \lim_{\Delta s \to 0} \frac{\varphi}{\Delta s} = \lim_{\Delta s \to 0} \frac{\frac{\Delta s}{R}}{\Delta s} = \frac{1}{R}. \quad \text{(B.4)}$$

Given any curve C and a point P on it, there is a unique circle, which approximates the curve near P the best, see Fig. B.5. The curvature of C at a point P is defined to be the curvature of that **circle of curvature** or reciprocal to the radius of that circle (**radius of curvature**).

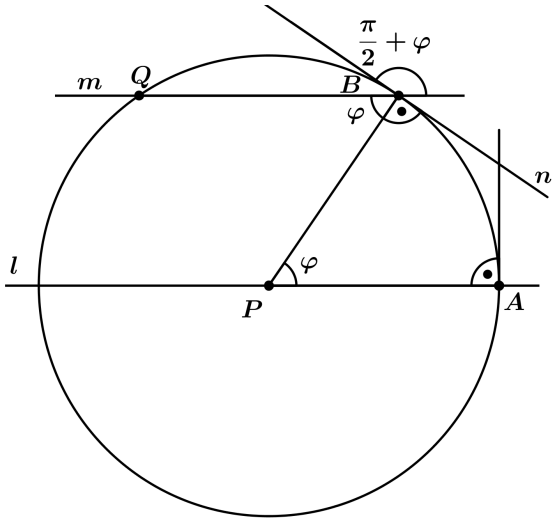

Figure B.4: The curvature of a circle is $k = \frac{1}{R}$.

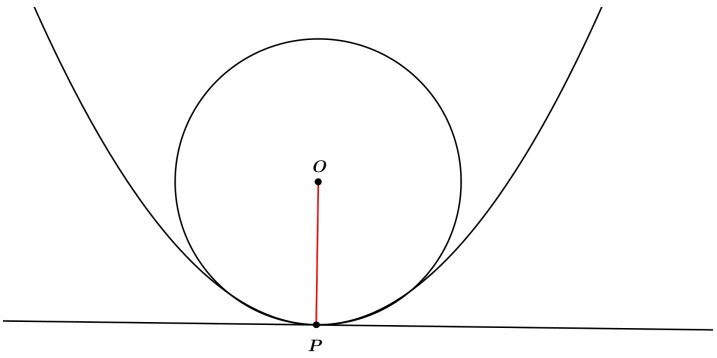

Figure B.5: Locally, the curvature of every point can be approximated with the curvature of a circle.

B.2 Surfaces

B.2.1 Tangent and normal vectors

Let us consider a surface $r(u, v)$. Let us consider two points $A = r(u + \Delta u, v)$ and $B = r(u, v)$ on the surface, see Fig. B.6. The vector $\overrightarrow{AB}$ is

$$\overrightarrow{AB} = r(u + \Delta u, v) - r(u, v) = \frac{r(u + \Delta u, v) - r(u, v)}{\Delta u}\Delta u.$$

If Δu tends to 0, i.e. the point B tends to the point A, then the direction of $\overrightarrow{AB}$ tends to the direction of the tangent vector r_u, where

$$r_u := \frac{\partial r}{\partial u} = \lim_{\Delta u \to 0} \frac{r(u + \Delta u, v) - r(u, v)}{\Delta u},$$

but $\overrightarrow{AB}$ and r_u are with different lengths. Analogously, r_v is tangent to the surface at the point A. The tangent vectors r_u and r_v span the tangent plain

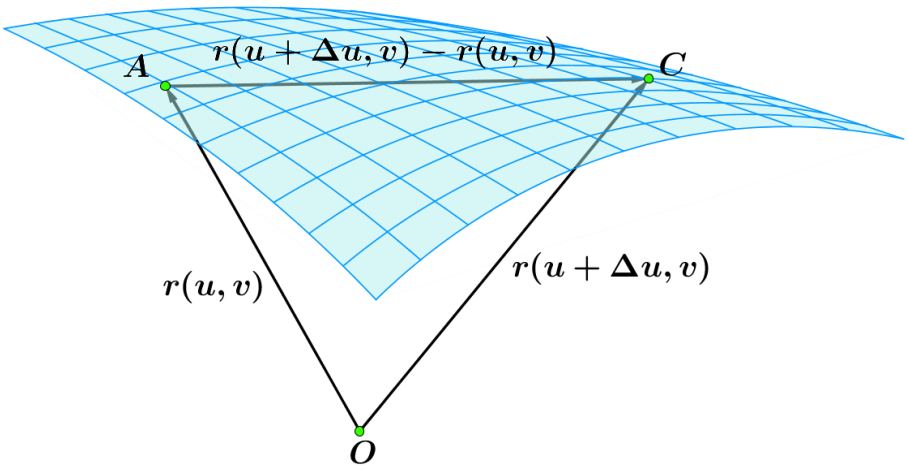

Figure B.6: $r(u+\Delta u)-r(u)$ tends to the tangent vector when $\Delta u \to 0$.

and every vector, which is their linear combination, lies in that plain. Therefore, the vector

$$\overrightarrow{PQ} = \frac{\partial r}{\partial u}du + \frac{\partial r}{\partial v}dv = r_u du + r_v dv, \tag{B.5}$$

is tangent to the surface. When P tends to Q, the length of the vector PQ tends to the length ds of the arc PQ, i.e

$$\lim_{P\to Q} ds = \lim_{P\to Q} |\vec{PQ}| = \sqrt{(r_u du + r_v dv)^2} = \sqrt{r_u^2(du)^2 + 2r_u r_v dudv + (r_v)^2} = \sqrt{E(du)^2 + 2Fdudv + G(dv)^2}, \tag{B.6}$$

where $E = r_u^2$, $F = r_u r_v$, $G = r_v^2$. Therefore, the unit tangent vector is

$$t = \frac{r_u du + r_v dv}{\sqrt{E(du)^2 + 2Fdudv + G(dv)^2}}.$$

Let us define the normal vector as

$$n = \frac{r_u \times r_v}{|r_u \times r_v|}.$$

Obviously, n is perpendicular to the tangent plane, i.e.

$$n \cdot t = 0.$$

B.2.2 Curvature

We want to calculate the normal curvature of the surface C at a point P. First, we can find a plain p through P, which is normal to C. The intersection of the plain p and the surface C is a plain curve with curvature k. There are infinitely many such plains p_i with curvatures k. There is a plain among them with minimal curvature k_{min} and a plain with maximal curvature k_{max} (k_{min}

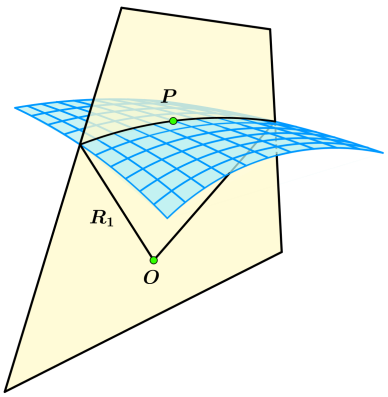

Figure B.7: k_{max}

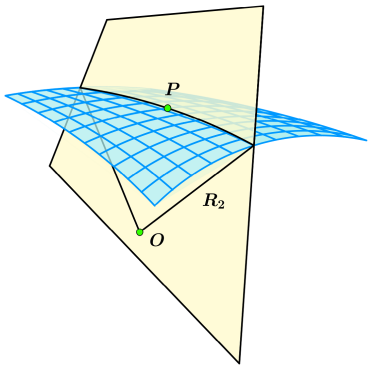

Figure B.8: k_{min}

and k_{max} are called **principal curvatures**). The mean curvature H is defined as the average of the principal curvatures or

$$H = \frac{k_{min} + k_{max}}{2}. \tag{B.7}$$

From (B.4) and (B.7) it follows that

$$H = \frac{1}{2}\left(\frac{1}{R_1} + \frac{1}{R_2}\right),$$

where R_1 and R_2 are the radii of the circles that best approximate the curvature of the curves, lying in normal planes through P. They are called **principal radii of curvature**. In order to compute the maximum and the minimum curvature, first we will find the curvature of a curve, parameterized with respect to the arc length, on the surface through the point P. For this purpose differentiating $n(s)t(s) = 0$ with respect to s, we obtain

$$\frac{dn}{ds}t + n\frac{dt}{ds} = 0 \;\Rightarrow\; n\frac{dt}{ds} = -\frac{dn}{ds}t.$$

Let us define the normal curvature as $k_n = kn$ and compute it

$$k_n = kn = n\frac{dt}{ds} = -\frac{dn}{ds}t = -\frac{dn}{ds}\frac{dr}{ds} = -\left(\frac{\partial n}{\partial u}\frac{du}{ds} + \frac{\partial n}{\partial v}\frac{dv}{ds}\right)\left(\frac{\partial r}{\partial u}\frac{du}{ds} + \frac{\partial r}{\partial v}\frac{dv}{ds}\right) =$$

$$= -n_u r_u \left(\frac{du}{ds}\right)^2 - (n_u r_v + n_v r_u)\frac{du}{ds}\frac{dv}{ds} - n_v r_v \left(\frac{dv}{ds}\right)^2 =$$

$$= -\frac{n_u r_u (du)^2 + (n_u r_v + n_v r_u)dudv + n_v r_v (dv)^2}{(ds)^2}$$

$$\overset{Eq.(B.6)}{=\!=} -\frac{n_u r_u (du)^2 + (n_u r_v + n_v r_u)dudv + n_v r_v (dv)^2}{r_u^2(du)^2 + 2r_u r_v dudv + r_v^2(dv)^2} = \frac{L(du)^2 + 2Mdudv + N(dv)^2}{E(du)^2 + 2Fdudv + G(dv)^2},$$

where $L = -r_u n_u$, $M = -\frac{1}{2}(r_u n_v + r_v n_u)$, $N = -r_v n_v$, $E = r_u^2$, $F = r_u r_v$, $G = r_v^2$. If we define $\lambda = \frac{dv}{du}$, then

$$k_n = \frac{L + 2M\lambda + N\lambda^2}{E + 2F\lambda + G\lambda^2} := f(\lambda).$$

In order to find k_{min} and k_{max}, we must find the extrema of $f(\lambda)$. We are looking for values of λ, such that

$$f'(\lambda) = \frac{(2M + 2N\lambda)(E + 2F\lambda + G\lambda^2) - (L + 2M\lambda + N\lambda^2)(2F + 2G\lambda)}{(E + F\lambda + G\lambda^2)^2} = 0$$

After short computations, we obtain

$$\frac{M + N\lambda}{F + G\lambda} = \frac{L + 2M\lambda + N\lambda^2}{E + 2F\lambda + G\lambda^2} = \frac{L + M\lambda + \lambda(M + N\lambda)}{E + F\lambda + \lambda(F + G\lambda)} = \frac{L + M\lambda}{E + F\lambda} = k_n. \tag{B.8}$$

Therefore

$$\lambda = \frac{k_n F - M}{N - k_n G} = \frac{Ek_n - L}{M - k_n F}.$$

holds true. Using the latter equation, we obtain a quadratic equation in k_n:

$$k_n^2(F^2 - GE) + (NE + GL - 2FM)k_n + M^2 - NL = 0.$$

The mean curvature is then

$$H = -\frac{NE + GL - 2FM}{2(F^2 - GE)}.$$

and it can be computed directly. We shall proof that the principal directions t_{min} and t_{max} are orthogonal. For this purpose we shall find their dot product:

$$\begin{aligned} t_{min}t_{max} &\overset{Eq.(B.5)}{=\!=} \left(\frac{\partial r}{\partial u}du_1 + \frac{\partial r}{\partial v}dv_1\right)\left(\frac{\partial r}{\partial u}du_2 + \frac{\partial r}{\partial v}dv_2\right) \\ &= (r_u)^2 du_1 du_2 + r_u r_v(du_1 dv_2 + du_2 dv_1) + (r_v)^2 dv_1 dv_2 \\ &= du_1 du_2 \left((r_u)^2 + r_u r_v\left(\frac{dv_2}{du_2} + \frac{dv_1}{du_1}\right) + (r_v)^2 \frac{dv_2}{du_2}\frac{dv_1}{du_1}\right) \end{aligned}$$

From the definition of the variables $E = r_u^2$, $F = r_u r_v$, $G = r_v^2$, $\lambda_{max} = \dfrac{dv_1}{du_1}$ and $\lambda_{min} = \dfrac{dv_2}{du_2}$, it is obvious that

$$t_{min}t_{max} = du_1 du_2 \left(E + F\left(\lambda_{min} + \lambda_{max}\right) + G\lambda_{min}\lambda_{max}\right). \tag{B.9}$$

From (B.9) we have that

$$(NF - GM)\lambda^2 + (NE - GL)\lambda + ME - FL = 0.$$

Using Vieta's formulas, we obtain

$$\begin{aligned} \lambda_{min} + \lambda_{max} &= \frac{GL - NE}{NF - GM} \\ \lambda_{min}\lambda_{max} &= \frac{ME - LF}{NF - GM}. \end{aligned}$$

Then we can substitute the latter equations in (B.9) and conclude that $t_{min}t_{max} = 0$, i.e. the tangents are orthogonal.

Bibliography

[1] M. Hoorfar, A. W. Neumann, Recent progress in axisymmetric drop shape analysis (ADSA), Advances in Colloid and Interface Science 121 (2006) 25-49.

[2] S. Dimova, T. Chernogorova, A. Iotova, Numerical Methods for Differential Equations, University press "St. Kl. Ohridski", Sofia, 2010 (in Bulgarian).

[3] Y. Rotenberg, L. Boruvka, A. W. Neumann, Determination of surface tension and contact angle from the shapes of axisymmetric fluid interfaces, Journal of Colloid and Interface Science 93 (1983) 169–183.

[4] O. I. del Rio, A. W. Neumann, Axisymmetric drop shape analysis: computational methods for the measurement of interfacial properties from the shape and dimensions of pendant and sessile drops of axisymmetric fluid interfaces, Journal of Colloid and Interface Science 196 (1997) 136-147.

[5] J. Casey, Exploring Curvature, Vieweg, 1st edition, 1996.

[6] `http://www.dynetechnology.co.uk/products/contact-angle-meter--tensiometer-cam001/` (up to date on October 22, 2015)

[7] `http://www.ebatco.com/interfacial_tension.html`(up to date on October 22, 2015)

[8] `http://www.alibaba.com/product-detail/TX500H-spinning-drop-interfacial-tensiometer_744901638.html`(up to date on October 22, 2015)

[9] `http://study.com/academy/lesson/capillary-action-of-water-definition-examples-lesson.html`(up to date on October 22, 2015)